The dual function monoclonal antibodies VIR-7831 and VIR-7832 demonstrate potent in vitro and in vivo activity against SARS-CoV-2

Andrea L. Cathcart[1], Colin Havenar-Daughton[1], Florian A. Lempp[1], Daphne Ma[1], Michael A. Schmid[2], Maria L. Agostini[1], Barbara Guarino[2], Julia Di iulio[1], Laura E. Rosen[1], Heather Tucker[1], Joshua Dillen[1], Sambhavi Subramanian[1], Barbara Sloan[1], Siro Bianchi[2], Dora Pinto[2], Christian Saliba[2], Katja Culap[2], Jason A Wojcechowskyj[1], Julia Noack[1], Jiayi Zhou[1], Hannah Kaiser[1], Arthur Chase[1], Martin Montiel-Ruiz[1], Exequiel Dellota Jr.[1], Arnold Park[1], Roberto Spreafico[1], Anna Sahakyan[1], Elvin J. Lauron[1], Nadine Czudnochowski[1], Elisabetta Cameroni[1], Sarah Ledoux[1], Adam Werts[3], Christophe Colas[1], Leah Soriaga[1], Amalio Telenti[1], Lisa A. Purcell[1], Seungmin Hwang[1], Gyorgy Snell[1], Herbert W. Virgin[1], Davide Corti[2], Christy M. Hebner[1*]

[1]Vir Biotechnology, San Francisco, California 94158, USA

[2]Humabs Biomed SA, a subsidiary of Vir Biotechnology, 6500 Bellinzona, Switzerland

[3]Lovelace Biomedical, Albuquerque, New Mexico 87108, USA

*corresponding author: chebner@vir.bio

ABSTRACT

Sotrovimab (VIR-7831) and VIR-7832 are dual action monoclonal antibodies (mAbs) targeting the spike glycoprotein of severe acute respiratory syndrome coronavirus 2 (SARS-CoV-2). Sotrovimab and VIR-7832 were derived from a parent antibody (S309) isolated from memory B cells of a 2003 severe acute respiratory syndrome coronavirus (SARS-CoV) survivor. Both mAbs contain an "LS" mutation in the Fc region to prolong serum half-life. In addition, VIR-7832 encodes an Fc GAALIE mutation that has been shown previously to evoke CD8+ T-cells in the context of an in vivo viral respiratory infection. Sotrovimab and VIR-7832 potently neutralize wild-type and variant pseudotyped viruses and authentic virus in vitro. In addition, they retain activity against monoclonal antibody resistance mutations conferring reduced susceptibility to previously authorized mAbs. The sotrovimab/VIR-7832 epitope continues to be highly conserved among circulating sequences consistent with the high barrier to resistance observed in vitro. Furthermore, both mAbs can recruit effector mechanisms in vitro that may contribute to clinical efficacy via elimination of infected host cells. In vitro studies with these mAbs demonstrated no enhancement of infection. In a Syrian Golden hamster proof-of concept wildtype SARS-CoV-2 infection model, animals treated with sotrovimab had less weight loss, and significantly decreased total viral load and infectious virus levels in the lung compared to a control mAb. Taken together, these data indicate that sotrovimab and VIR-7832 are key agents in the fight against COVID-19.

INTRODUCTION

The coronavirus disease (COVID-19) pandemic caused by severe acute respiratory syndrome coronavirus 2 (SARS-CoV-2) has resulted in nearly 400 million confirmed cases and over 5.7 million deaths worldwide[1]. SARS-CoV-2 infection results in a broad range of disease severity[2]. Infection fatality rates increase significantly with age, with 28.3% of COVID-19 patients over the age of 85 succumbing to

47 disease[2]. However, even in mild-to-moderate COVID-19 patients, significant post-infection sequelae can
48 affect overall health and cause long-term disability[3]. While multiple SARS-CoV-2 vaccines are now
49 available for use, issues of supply, vaccine hesitancy and emergence of variants may prevent rapid
50 attainment of herd immunity[4–9]. In addition, there are individuals who remain at risk despite vaccination
51 due to disease or underlying immunodeficiency. Thus, additional interventions and potential prophylactic
52 agents are needed to reduce morbidity and mortality due to COVID-19.

53 Over the course of the pandemic, multiple monoclonal antibodies (mAbs) targeting the SARS-CoV-2
54 spike protein have been authorized or approved for use in early treatment of COVID-19 patients[10–13] .
55 However, many of these agents are ineffective against the currently circulating Omicron variant,
56 especially those antibodies that target the receptor binding motif (RBM) of the viral spike (S)
57 glycoprotein[14–16]. Antibodies targeting highly conserved epitopes outside of the RBM may potentially
58 long-term better retain activity against ever-emerging SARS-CoV-2 variants. Furthermore, in addition to
59 viral neutralization, antibodies possessing potent effector function to aid in the killing of virally infected
60 cells and the elicitation of T cell immunity could additionally assist in halting disease progression[17–19].

61 Sotrovimab and VIR-7832 are dual action mAbs derived from the parent antibody S309 identified from a
62 2003 SARS-CoV survivor[20]. These mAbs target an epitope containing a glycan (at position N343) that is
63 highly conserved within the Sarbecovirus subgenus in a region of the S receptor binding domain (RBD)
64 that does not compete with angiotensin converting enzyme 2 (ACE2) binding[21]. The variable region of
65 sotrovimab and VIR-7832 have been engineered for enhanced developability. In addition, both antibodies
66 possess an Fc "LS" mutation that confers extended half-life by binding to the neonatal Fc receptor[22–24].
67 VIR-7832 is identical to sotrovimab with the exception of the addition of a 3 amino acid GAALIE
68 (G236A, A330L, I332E) modification to the Fc domain[25]. The GAALIE modification has previously been
69 shown in vitro to enhance binding to FcγIIa and FcγIIIa receptors, decrease affinity for FcγIIb compared
70 to typical IgG1 and evoke protective CD8+ T-cells in the context of viral respiratory infection in vivo
71 [26,27].

72 Here we characterize the antiviral activity of sotrovimab and VIR-7832. These mAbs effectively
73 neutralize SARS-CoV-2 live virus in vitro as well as in pseudotyped virus assays against emerging
74 variants of concern and variants that confer resistance to previously authorized or approved mAbs[28]. In
75 addition to the neutralizing capacity, both antibodies demonstrate potent effector function and mediate
76 antibody dependent cellular cytotoxicity (ADCC) and antibody dependent cellular phagocytosis (ADCP)
77 in vitro. Furthermore, resistance selection experiments and epitope conservation analyses indicate the
78 potential for a high barrier to resistance. Data derived from the Syrian golden hamster model
79 demonstrates efficacy in a proof-of-concept in vivo model. Taken together, these data indicate that
80 sotrovimab and VIR-7832 are key components of the arsenal in the fight against COVID-19.

81 **RESULTS**

82 **Sotrovimab and VIR-7832 bind SARS-CoV-2 spike and effectively neutralize live virus in vitro.**
83 Previously published work showed that S309 bound SARS-CoV-2 recombinant and cell surface-
84 associated S and neutralized live virus in vitro[20]. We initiated these studies by repeating and extending
85 these earlier results. To determine the binding activity of sotrovimab and VIR-7832 to the SARS-CoV-2
86 S, enzyme-linked immunosorbent assay (ELISA), surface plasmon resonance (SPR) and flow cytometry
87 assays were utilized. Sotrovimab and VIR-7832 bound to recombinant S RBD (amino acids 331-541)
88 with EC_{50} values of 20.40 ng/mL and 14.9 ng/mL, respectively, by ELISA (**Figure 1a**). Using SPR, both
89 antibodies demonstrated potent binding to recombinant S RBD with an equilibrium constant (Kd) of 0.21
90 nM (**Figure 1b**). As antibody recognition of cell surface-bound S could mediate killing of virally infected
91 cells, flow cytometry-based studies using cells transiently transfected with a S-encoding plasmid were
92 used to examine antibody binding to cell surface-expressed S trimer. By this method, both sotrovimab and
93 VIR-7832 bound efficiently to surface-expressed S (**Figure 1c**).

94 To examine neutralization capacity, sotrovimab and VIR-7832 were tested in a VeroE6 cell-based live
95 SARS-CoV-2 virus system against the Washington 2019 (wild-type) virus as well as against the Alpha
96 (B.1.1.7), Beta (B.1.351), Gamma (P.1), Delta (B.1.617.2) and Kappa (B.1.617.1) variants.

97 Concentration-dependent viral neutralization of the Washington 2019 strain was observed for both
98 antibodies, with geometric mean $IC_{50/90}$ values of 100.1/186.3 ng/mL and 78.3/253.1 ng/mL, respectively
99 (**Figure 1d**). $IC_{50/90}$ values observed for sotrovimab and VIR-7832 against the Beta, Gamma, Delta and
100 Kappa variant viruses were similar to those against the wild-type strain. A slight shift in the
101 sotrovimab/VIR-7832 $IC_{50/90}$ compared to wild-type was observed for the Alpha variant. Sotrovimab
102 showed a 3-fold and 4.1-fold shift in IC_{50} and IC_{90}, respectively, against the Alpha variant compared to
103 wild-type while VIR-7832 had a 3.1-fold shift in IC_{50} and 3.7-fold shift in IC_{90} versus wild-type (**Figure**
104 **1d, Table 1)**. As variant evolution is a natural part of SARS-CoV-2 biology and emerging live virus
105 variants are not always readily accessible for testing, a vesicular stomatitis virus (VSV)-based
106 pseudotyped virus system targeting Vero E6 cells was used to examine sotrovimab and VIR-7832
107 neutralization against emergent variants (**Table 2**). Fold-changes in sotrovimab and VIR-7832 IC_{50} values
108 compared to wild-type against pseudotyped virus expressing spike from the Alpha, Beta, Gamma, Delta
109 and Kappa variants were similar to those observed in the authentic virus system. Sotrovimab was tested
110 against an extended panel of pseudotyped viruses incorporating emerging variants as well as variants
111 currently or previously deemed as Variants of Concern (VOC) or Variants of Interest (VOI) by the World
112 Health Organization (WHO). Sotrovimab neutralized all variants tested with fold changes in IC_{50}s of
113 ≤3.3-fold observed for 21 of 22 variants assessed (**Table 2**), while a 16-fold change in IC_{50} was observed
114 for the Omicron BA.2 variant (**Table 2, Figure 1e**).

115 **Sotrovimab and VIR-7832 exhibit potent effector function in vitro.** Although direct antiviral
116 mechanisms are crucial to provide protection, Fc-dependent mechanisms mediated by interaction with Fc
117 gamma receptors (FcγRs) on immune cells or with complement, can contribute to overall potency in vivo.
118 The potential for sotrovimab and VIR-7832 to mediate effector functions were assessed in vitro by
119 measuring binding to FcγRs and C1q and in assays designed to demonstrate antibody-dependent cellular
120 cytotoxicity (ADCC) or antibody-dependent cellular phagocytosis (ADCP)[29–32].

121 Antibody binding to the human activating FcγRIIa (low-affinity R131 and high affinity H131 alleles),
122 FcγRIIIa (low-affinity F158 and high-affinity V158 alleles), and to the inhibitory FcγRIIb were examined
123 using SPR (**Supplemental figure 1a**). Sotrovimab similarly bound both the H131 and R131 alleles of
124 FcγRIIa and binds FcγRIIb. Sotrovimab bound both FcγRIIIa alleles, with reduced binding to the F158
125 allele compared to V158, as is characteristic for human IgG1[33]. Binding of sotrovimab to C1q was similar
126 to the parental antibody (S309-LS) (**Supplemental figure 1b**). As previously reported for antibodies
127 encoding the GAALIE mutation[25,34], VIR-7832 bound with comparatively higher affinity to activating
128 FcγRIIa and FcγRIIIa than sotrovimab (**Supplemental figure 1a**). Conversely, VIR-7832 showed
129 reduced affinity for FcγIIb and abrogation of binding to C1q (**Supplemental figure 1b**).

130 The antibodies were also assessed for the ability to activate human FcγRIIa, FcγRIIb or FcγRIIIa, using a
131 Jurkat cell reporter assay[35] (**Figure 2a-d**). S309-GRLR, which contains the effector function-abrogating
132 G236R, L328R mutations was used as a negative control. Cells stably transfected with the SARS-CoV-2
133 spike protein (CHO-CoV-2-Spike) served as target cells. Both sotrovimab and the parental S309-LS
134 activated signaling of the higher-affinity allele FcγRIIa (H131) but did so less efficiently than the
135 GAALIE-containing antibody VIR-7832 (**Figure 2a**) while sotrovimab, VIR-7832 and S309-LS induced
136 similar low-level activation of the inhibitory receptor FcγRIIb (**Figure 2b**). Sotrovimab demonstrated
137 substantially lower activation of FcγRIIIa F158 versus V158 as expected while VIR-7832 showed
138 increased activation of both alleles of FcγRIIIa (F158 and V158) (**Figures 2c,d**).

139 To further elucidate the effector function potential of the antibodies, ADCC and ADCP assays were
140 performed using donor PBMCs or NK cells as effector cells and CHO cells stably expressing S (CHO-
141 CoV-2-Spike) as target cells (**Figure 2e-g**). The ability of antibodies to activate NK cell-mediated killing
142 was measured in vitro using two genotyped donors expressing homozygous low-affinity (F/F158) or high-
143 affinity (V/V158) (**Figure 2e-f**). Compared to the parental mAb S309-LS, sotrovimab had slightly
144 increased capacity to induce NK cell-mediated ADCC when using cells from either F/F158 or V/V158
145 donors. As expected, VIR-7832 induced NK cell-mediated ADCC in cells from donors expressing the

146 low-affinity F/F158 allele of FcγIIIa more efficiently than VIR-7831. These results were confirmed with
147 NK cells from a heterozygous donor (F/V158).

148 The ability of sotrovimab and VIR-7832 to facilitate ADCP by primary $CD14^+$ monocytes was measured
149 in vitro by exposing freshly isolated human PBMCs to CHO-CoV-2-Spike cells that were pre-incubated
150 with antibody (**Figure 2g**). Sotrovimab, VIR-7832 and S309-LS induced similar levels of ADCP by
151 $CD14^+$ monocytes. These results indicate that sotrovimab and VIR-7832 have the potential to trigger
152 ADCC and ADCP of cells displaying SARS CoV-2 S protein.

153 **Subneutralizing levels of sotrovimab and VIR-7832 do not enhance virus uptake, replication or**
154 **cytokine production in vitro.** One potential concern with any antibody therapeutic targeting a viral agent
155 is the possibility of antibody-dependent enhancement (ADE). ADE is an in vivo phenomenon in which
156 the presence of an antibody worsens disease. There are several in vitro assays that may provide plausible
157 correlates for ADE in vivo, though none of these have been proven relevant to COVID-19 as to date ADE
158 has not been observed in trials of monoclonal antibodies or plasma[13,36–38]. ADE can occur by several
159 potential mechanisms[39]. Poorly neutralizing antibodies or subneutralizing levels of antibody could
160 theoretically facilitate enhanced virus entry and infection through Fc receptor interactions. A second
161 theoretical mechanism involves antibody-antigen complex formation leading to enhanced cytokine
162 production. A third mechanism of ADE has been observed in a porcine model of influenza where the
163 kinetics of viral fusion to the target cell was enhanced in a Fab-dependent manner by fusion-enhancing
164 non-neutralizing antibodies[40,41].

165 To explore whether sotrovimab and VIR-7832 exhibit in vitro activities that might be related to ADE in
166 vivo, we evaluated SARS-CoV-2 replication in human cells that express FcγRs: monocyte-derived
167 dendritic cells (moDCs), peripheral blood mononuclear cells (PBMCs) and the human U937 macrophage
168 cell line (**Supplemental Figure 2a-b**). Subneutralizing concentrations of sotrovimab and VIR-7832 were
169 precomplexed with SARS-CoV-2 (MOI =0.01) and added to target cells. Using immunostaining methods,
170 at 24 hours post-infection no productive entry of SARS-CoV-2 into moDCs, PBMCs, or U937 cells was

171 observed in the presence or absence of either mAb, while VeroE6 control cells demonstrated
172 internalization in all conditions evaluated. Reduced internalization of SARS-CoV-2 in VeroE6 cells was
173 observed at the highest concentration of sotrovimab and VIR-7832 (p-value <0.05), indicating effective
174 virus neutralization prevented virus entry. Using a focus forming assay, virus replication and secretion of
175 infectious virus were detectable by 48 hours post-infection in VeroE6 cells, with comparable levels of
176 replication in the presence or absence of sotrovimab or VIR-7832. However, no replication of SARS-
177 CoV-2 was detected in moDCs, PBMCs or U937 cells regardless of antibody treatment, indicating lack of
178 productive SARS-CoV-2 infection of these cells, consistent with previously published data[42].

179 To evaluate the potential for sotrovimab and VIR-7832 to enhance cytokine release upon SARS-CoV-2
180 infection in FcγR-expressing cells, cytokines and chemokines were measured in the supernatants from
181 cells infected with SARS-CoV-2-in the presence of sotrovimab or VIR-7832 (**Supplemental figure 2c**).
182 Levels of IFN-γ, IL-10, IL-6, IL 8, IP-10, MCP-1, and TNF-α in the supernatant were quantified by MSD
183 at 24- and 48-hours post-infection. For all cell types evaluated, cytokine/chemokine production was
184 similar between all antibody concentrations tested and the no antibody control at both 24- and 48-hours
185 post-infection. Taken together, these in vitro data indicate that neither VIR-7831 nor VIR-7832 exhibit in
186 vitro activities that have been proposed to possibly correlate with ADE in vivo.

187 **Sotrovimab and VIR-7832 have a high barrier to resistance in vitro and do not display cross-**
188 **resistance with other SARS-CoV-2 mAbs.** We next determined whether resistant variants could be
189 elicited by serial passage of SARS-CoV-2 in the presence of VIR-7832. As sotrovimab and VIR-7832
190 differ only in the Fc region of the antibody, resistance selection experiments were conducted with VIR-
191 7832 as a proxy for both antibodies. SARS-CoV-2 was subjected to 10 passages in the presence of VIR-
192 7832 at fixed concentrations of ~10x, 20x, 50x or 100x IC_{50} (1, 2, 5, or 10 μg/mL) in VeroE6 cells. No
193 CPE was detected in wells passaged with antibody through 10 passages, while CPE was observed in the
194 no antibody control in all passages. Similarly, no virus was detected by focus forming assay at any
195 concentration of VIR-7832 through all 10 passages even at the lowest concentration tested.

196 As no viral breakthrough was observed in the fixed concentration resistance selection, a second method
197 was employed wherein SARS-CoV-2 virus was passaged in sub-IC_{50} concentrations of antibody followed
198 by subsequent passaging in the presence of increasing concentrations of mAb in an attempt to force
199 resistance emergence (**Supplemental Figure 3**). Passaging was performed in duplicate wells to account
200 for founder effects, and concentration increases for each well were based on CPE observations. Five
201 sequential passages were conducted using increasing concentrations of VIR-7832 at 0.5, 1, 2, 5 and ~10x
202 IC_{50} (0.05, 0.1, 0.2, 0.5, 1 μg/mL; **Supplemental Figure 3a**), though no CPE was observed by passages 4
203 and 5 (0.5 and 1 μg/mL, respectively) indicating that variants originally selected at the lower
204 concentrations were either unfit or susceptible to the higher concentrations of antibody. To further assess
205 whether resistance mutations could be generated, selection was restarted using passage 3 virus generated
206 with ~2x IC_{50} (0.2 μg/mL) of VIR-7832 in duplicate wells at ~2x and ~5x IC_{50} (0.2, 0.5 μg/mL),
207 generating two passage lineages (**Supplemental Figure 3b-c**).

208 Supernatants were evaluated for detectable virus at each passage by focus forming assay and cell
209 supernatants from viral passages containing detectable virus were tested in SARS-CoV-2 neutralization
210 assays to evaluate IC_{50} shifts as a marker of reduced susceptibility (**Supplemental Table 1**). With the
211 exception of passage 8, modest fold changes were observed, with shifts in IC_{50} values ranging from 5.4-
212 to 6.5-fold compared to the wild-type SARS-CoV-2 stock virus. In lineage 1, the passage 8 virus
213 displayed a >10-fold shift in IC_{50} (greater than highest concentration tested). Sequence analysis detected
214 an identical 4 amino acid insertion in the N-terminal domain (215-216insKLRS) and 5 amino acid
215 deletion in correspondence of the furin cleavage site (675-679del) in both lineages at all passages
216 sequenced, as well as the amino acid substitution E340A in lineage 1, and R682W, and V1128F in
217 lineage 2. The deletion at amino acids 675-679 has been previously described during passaging of SARS-
218 CoV-2 in tissue culture suggesting enrichment to be a result of cell culture adaptation[43] while the 215-
219 216insKLRS was detected in the input virus. Neither 215-216insKLRS nor R682W variants were highly
220 enriched with passaging (**Supplemental Table 1**) and enrichment of 675-679del and V1128F did not

221 profoundly alter the VIR-7832 IC_{50}. However, appearance of the E340A variant at 98.7% did correlate
222 with a >10-fold shift in IC_{50} suggesting this variant may confer resistance.

223 To evaluate whether amino acid variants identified in the resistance selection conferred reduced
224 susceptibility to sotrovimab and VIR-7832, neutralization of pseudotyped viruses encoding the S variants
225 was assessed (**Supplemental Table 2**). Sotrovimab and VIR-7832 neutralized R682W and V1128F
226 SARS-CoV-2 pseudotyped virus spike variants with IC_{50} values similar to wild type (< 2-fold change in
227 IC_{50}) indicating that these variants do not alter susceptibility. In contrast, E340A conferred reduced
228 susceptibility to VIR-7831 and VIR-7832 (> 100-fold change in IC_{50}) indicating that E340A is a VIR-
229 7831/VIR-7832 monoclonal antibody resistance mutation (MARM).

230 As sotrovimab /VIR-7832 demonstrated a unique in vitro resistance profile, we investigated the potential
231 for cross-resistance to MARMs that confer reduced susceptibility to the monoclonal antibodies
232 bamlanivimab, imdevimab and casirivimab [10,11,44–46] using pseudotyped virus. Notably, some of these
233 mutations are found in highly prevalent variants of concern[47–49]. Sotrovimab effectively neutralized
234 pseudotyped viruses expressing spike MARMs that alter bamlanivimab, casirivimab and/or imdevimab
235 activity (**Table 3**). Fold changes in IC_{50} values compared to wild-type were <3-fold for 18/19 variants
236 tested. A modest 3.4-fold shift in the sotrovimab IC_{50} was observed for the V445A variant that confers
237 reduced susceptibility to imdevimab. These data indicate that sotrovimab/VIR-7832 does not display
238 cross-resistance with currently authorized mAbs and supports the potential combination use of
239 sotrovimab/VIR-7832 with other mAb therapeutics.

240 **The sotrovimab/VIR-7832 epitope is highly conserved among SARS-CoV-2 sequences.** The parental
241 antibody of sotrovimab and VIR-7832 (S309) binds to a highly conserved sarbecovirus epitope that is
242 potentially intolerant of variation. To investigate the current state of epitope conservation, >4,500,000
243 spike sequences from SARS-CoV-2 deposited in the GISAID database as of November 11, 2021 were
244 examined for epitope variation. More than 99.6% conservation is seen for those amino acids comprising

245 the epitope among currently available sequences for all positions including 15/23 amino acid positions
246 that were ≥99.99 conserved (**Table 4**).

247 Sotrovimab activity against viral mutants carrying single substitutions in the epitope was assessed in
248 pseudotyped virus assays. VIR-7831 effectively neutralized epitope variants at most amino acid positions
249 tested (Supplemental **Table 5**). A moderate shift in activity was observed for the K356T variant (5.9-fold
250 shift in IC_{50}). Variants at two positions, E340 and P337, resulted in significant IC_{50} shifts indicating
251 reduced susceptibility to VIR-7831. Moderate shifts in potency were observed for P337H, P337T and
252 E340G substitutions (5.13-, 10.62- and 18.21-fold, respectively) while more significant shifts in potency
253 were observed for P337L/R/K and E340A/K/Q (at least >50-fold). Notably, these variants are detected in
254 a low number of sequences and do not have a pattern that suggest emergence in the GISAID database
255 (296 and 223 variant counts out of >4,500,000 sequences for P337 and E340, respectively). This
256 observation is consistent with the possibility that substitutions at these positions come with a fitness cost
257 to the virus.

258 **Sotrovimab reduces weight loss, total viral load and infectious virus levels in a hamster model of**
259 **SARS-CoV-2 infection.** To evaluate the efficacy of sotrovimab in vivo, the hamster model was utilized.
260 As it was unknown what effect the LS mutation would have in the hamster, a non-LS version of
261 sotrovimab (SGHmAb-no-LS) was used for these experiments. Hamsters were administered SGHmAb-
262 no-LS intraperitoneally at Day -1 (30, 5, 0.5 or 0.05 mg/kg) or Day -2 (15, 5, 0.5 or 0.05 mg/kg) prior to
263 intranasal SARS-CoV-2 inoculation (**Figure 3a**). Using body weight as a marker of degree of clinical
264 disease, doses of ≥5mg/kg resulted in significantly reduced weight loss at Day 4 compared to controls.
265 (**Figure 3b-e**). Significant decreases in lung viral load were also observed at ≥5mg/kg as measured by
266 RT-qPCR (**Figures 3f-g**). Day 4 $TCID_{50}$ measurements indicated that antibody administered at ≥0.5
267 mg/kg resulted in significantly lower levels of infectious virus in lung tissue compared to controls
268 (**Figure 3h-i**). Notably, across these experiments, no enhancement of disease was observed in animals
269 receiving SGHmAb-no-LS based on changes in weight, viral RNA in the lungs, or $TCID_{50}$ infectious

270 virus levels. Collectively, these data indicate that sotrovimab prevented in a dose-dependent fashion virus
271 replication and morbidity in SARS-CoV-2 challenged hamsters without signs of ADE at any dose tested.

272 **DISCUSSION**

273 Here we show the in vitro and in vivo preclinical characterization of sotrovimab and VIR-7832[50–52]. Both
274 antibodies demonstrate high-affinity binding to S in vitro, including on the surface of cells, and
275 effectively neutralize wildtype SARS-CoV-2 in a live virus assay. Sotrovimab and VIR-7832 retain
276 activity against the Alpha (B.1.1.7), Beta (B.1.351), Gamma (P.1), Delta (B.1.617.2) and Kappa
277 (B.1.617.1) variants in an authentic virus system and neutralize all pseudotyped virus variants tested.
278 Preclinical studies indicate neutralization alone is unlikely to fully describe the activity of antibodies like
279 sotrovimab, that retain effector function[17]. Sotrovimab also binds C1q, activate FcγRs and demonstrate
280 ADCC and ADCP in vitro. In addition, dose and pharmacokinetics are also important factors for clinical
281 activity. Experiments in the hamster model of SARS-CoV-2 infection show proof-of-concept efficacy in
282 vivo. Notably, in vitro and in vivo data did not provide any supporting evidence that these antibodies
283 would demonstrate ADE in a clinical setting.

284 That sotrovimab and VIR-7832 continue to neutralize spike variants in authentic virus and pseudotyped
285 virus assays is a key finding at this stage of the pandemic. With the increased transmissibility and
286 potential for more severe disease observed with these viruses, the availability of therapeutic or
287 prophylactic mAbs that remains active against variants is essential. Sotrovimab neutralized 21 of 22
288 variants tested with a fold-change in IC_{50} of ≤3.3-fold, including the Omicron BA.1 and BA.1.1
289 sublineages. A moderate shift in activity (16-fold change in IC_{50}) was observed for the Omicron BA.2
290 variant. In addition to neutralizing circulating variants, in pseudotyped virus experiments sotrovimab
291 showed no significant cross-resistance with variants that reduce the activity of previously authorized or
292 approved mAbs. These data additionally demonstrate the uniqueness of sotrovimab and VIR-7832 and
293 further highlight the utility sotrovimab and VIR-7832 have as clinical agents.

294 The sotrovimab/VIR-7832 epitope remains highly conserved among available sequences of circulating
295 virus with ≥99.66% conservation of epitope amino acids. This is consistent with the value of the strategy
296 used for isolation of monoclonal antibodies that neutralize both SARS-CoV and SARS-CoV-2 based on
297 the idea that these two virulent human viruses are phylogenetically divergent within the sarbecovirus
298 subgenus. Furthermore, MARMs identified at positions P337 and E340 are present at very low levels
299 among current sequences. That amino acids P337 and E340 remain ≥99.99% conserved at this stage of
300 the pandemic indicates that variants at these positions may confer disadvantageous effects on the virus,
301 consistent with the conservation of this epitope across the sarbecovirus family[20].

302 Viral variants of concern for RBM-targeting mAbs are quickly spreading[53]. The vaccines presently being
303 deployed around the world generate high-titer neutralizing antibodies that target the S protein RBM.
304 Importantly, the RBM is highly immunodominant for responses to natural infection[54]. Vaccine-induced
305 and convalescent immunity may therefore potentially put further mutational pressure on the RBM
306 sequence to evade such antibody responses. In contrast, antibody responses overlapping with the
307 sotrovimab/VIR-7832 epitope are limited after infection [54], possibly because of the shielding effect of the
308 highly conserved N343 glycan. In this regard the epitope may face less vaccine- or infection-generated
309 immune pressure, potentially preserving this conserved epitope long-term.

310 Recent data have indicated that the cells used to generate live virus stocks and overexpression of
311 ACE2/TMPRSS2 in target cells used for assays can affect mAb activity in vitro[28,55]. The
312 sotrovimab/VIR-7832 parental antibody S309 seems particularly sensitive to in vitro methods using
313 ACE2 overexpressing cells[55]. It is therefore notable that sotrovimab displays significant efficacy in an in
314 vivo proof-of-concept SARS-CoV-2 infection experiment using hamsters despite the fact that patterns of
315 engagement of hamster FcRs by human IgG1 antibodies may not reflect patterns of human IgG1
316 antibodies with their cognate human FcRs. These findings argue that in vitro data derived from such
317 ACE2 and/or TMPRSS2 overexpression cell lines do not accurately reflect the in vivo antiviral capacity
318 of tested mAbs. Furthermore, that the significant in vivo effects of sotrovimab in the hamster model likely

occurred in the absence of full effector functions due to species-specific interactions between antibodies and FcRs, argues that effects in COVID-19 patients incorporating both the neutralization capacity of the antibody plus the ability to harness the strength of the immune system could lead to positive clinical outcomes.

The clinical potential of VIR-7832, with the inclusion of the GAALIE Fc mutation, is of special interest in the context of SARS-CoV-2 infection. Previously published data by the Ravetch laboratory comparing the in vivo efficacy of a hemagglutinin-targeting mAb with and without inclusion of the GAALIE mutation in a transgenic humanized FcγR mouse model of influenza infection demonstrated superior efficacy of the GAALIE-containing antibody in both therapeutic and prophylactic experiments[25]. These effects were mediated by protective $CD8^+$ T cell responses elicited by the GAALIE antibody. Clinical data examining the contribution of the adaptive immune response in SARS-CoV-2 infection indicate that poor T cell induction correlates with severe disease (reviewed in [56]). Thus, the potential for VIR-7832 to augment the T cell response to SARS-CoV-2 infection could conceivably play a crucial role in limiting progression to severe COVID-19 disease or in treatment of severe established disease. This latter possibility is supported by recent publications showing that monoclonal antibodies with effector functions are especially effective in the therapeutic setting via recruitment of tissue-protective monocyte functions [18], and that potency of antibodies in the pre-clinical mouse model does not correlate with in vitro neutralizing activity of antibodies[17].

Taken together, these data indicate that sotrovimab and VIR-7832 play a powerful role in the fight against COVID-19 through the dual action of broadly neutralizing activity paired with engagement of the immune system through effector function capabilities.

METHODS

342 **Cells.** Vero E6 cells (ATCC) and Lenti-X 293T cells (Takara) were cultured in Dulbecco's Modified
343 Eagle's medium (DMEM), 10% FBS, 1x Penicillin-Streptomycin at 37°C, 5% CO_2.

344 **Monoclonal Antibodies.** Sotrovimab (VIR-7831) and VIR-7832 were produced at WuXi Biologics
345 (China). SGHmAb-no-LS, S309-LS, and S309-GRLR were produced at Humabs Biomed SA, a
346 subsidiary of Vir Biotechnology (Bellinzona, Switzerland) in expiCHO cells transiently co-transfected
347 with plasmids expressing the heavy and light chain, as previously described [57]

348 **Virus. S**ARS-CoV-2 isolates USA-WA1/2020, UK/VUI/3/2020, hCoV-19/South Africa/KRISP-
349 K005325/2020, hCoV-19/Japan/TY7-503/2021, hCoV-19/USA/CA-SU-15-S02/2021 and hCoV-
350 19/USA/PHC658/2021 were obtained from BEI Resources. To propagate SARS-CoV-2, VeroE6 or
351 VeroE6-TMPRSS2 cells were seeded at $10X10^6$ cells in T175 flasks in growth media and infected the
352 next day at a MOI of 0.001 in virus propagation media. Virus was adsorbed for 1 hour at 37°C. Virus
353 inoculum was removed, flasks were washed once with PBS, 25 mL of infection media was added to the
354 cells and flasks were incubated at 37°C. Supernatants were collected at 48 hours post-infection once
355 cytopathic effect was visible, centrifuged at 500 x g for 5 minutes, followed by a second centrifugation at
356 1000 x g for 5 minutes. Clarified supernatants were then aliquoted and stored at -80°C. Virus titers were
357 determined using a plaque assay on VeroE6 cells, using standard methods. Briefly, 10-fold dilutions of
358 virus stock were incubated in 6 well plates with 2.4% colloidal cellulose overlay for 24 hours. Cells were
359 fixed with 4% PFA for 30 minutes at room temperature (RT), permeabilized with 0.125% Triton X-100,
360 stained with anti-SARS-CoV-2 nucleocapsid antibody at 1:5000 and goat anti-rabbit IgG HRP at 1:5000.
361 Plaque forming units (PFU) were visualized with TrueBlue reagent.

362 **In vitro binding ELISA.** For the ELISA assay, 96-well plates were coated with 100 µl/well recombinant
363 SARS-CoV2 RBD diluted in assay diluent (1% BSA/PBS) at a final concentration of 2 µg/mL and
364 incubated overnight at 4°C. Plates were washed three times with 300 µl/well wash buffer using an
365 automated washer. Assay diluent (100 µl/well) was added to block the plates and incubated for 1 hour at
366 room temperature (RT) with shaking. Assay diluent was removed, and plates washed three times with

367 wash buffer. Serial 1:3 dilutions of mAb (concentration range from 6 µg/mL to 0.33 ng/mL) in assay
368 diluent were dispensed at 100 µl/well and incubated 1 hour at RT with shaking, then washed three times
369 with wash buffer. The HRP-conjugated secondary antibody reagent (1:5,000 dilution in assay diluent)
370 was added to each well (100 µl/well) and incubated for 1 hour at RT with shaking. After three washes
371 with wash buffer, 100 µl/well of 2-component TMB peroxidase substrate solution was dispensed in each
372 well and developed for 5 minutes at RT. The reaction was stopped with 100 µL/well 1M H_2SO_4 and the
373 OD was read immediately at 450 nm on a SpectraMax M5 Microplate reader. EC_{50} values were calculated
374 using non-linear regression of log (agonist) versus response in Graph Pad Prism.

375 **Spike binding affinity quantification by SPR.** Antibody was diluted to 2 µg/mL (1 mL) in HBS-EP+
376 buffer and injected at 10 µL/min for 30 seconds across one flow cell of a CM5 sensor chip immobilized
377 with anti-human Fc antibody docked in a Biacore T200. SARS-CoV2-RBD diluted in HBS-EP+ buffer
378 was then injected at a single concentration, 1:3 dilutions from 100 nM to 3.7 nM, across both the flow cell
379 containing captured the antibody as well as a reference flow cell containing only anti-human Fc antibody.
380 Binding was measured with a flow rate of 30 µL/min and an injection time of 600 seconds; dissociation
381 was monitored for 1800 seconds after injection. Data were collected at 10 Hz. After each binding
382 measurement, regeneration reagent was injected to prepare the surface for a new cycle. Experiments were
383 performed at 25°C, with the samples held at 15 °C in the instrument prior to injection.

384 **Measurement of Binding to Human Fcγ Receptors by SPR.** Binding of sotrovimab and VIR-7832 to
385 human recombinant FcγRs was measured by surface plasmon resonance (SPR) on a Biacore T200.
386 Briefly, Biotin CAPture Reagent (modified streptavidin) was injected across all flow cells of a CAP
387 sensor chip docked in a Biacore T200. Biotinylated Fc receptors at 1 µg/mL were injected across a single
388 flow cell at 10 µL/min for 60 seconds (one receptor per flow cell), with one flow cell reserved as a
389 reference surface. VIR 7831 or VIR-7832 at 100 µg/mL (diluted in HBS-EP+) were injected across all
390 flow cells for 200 seconds using a flow rate of 30 µL/min and association was monitored. Dissociation
391 was monitored for another 200 seconds after injection. Data was collected at 10 Hz. After each binding

392 measurement, CAP Regeneration reagent was injected to prepare the surface for a new cycle.
393 Experiments were performed at 25°C, with the samples held at 15°C in the instrument prior to injection.

394 **Measurement of Binding to Human Complement Protein C1q.** Binding of sotrovimab and VIR-7832
395 to human complement was measured by biolayer interferometry (BLI) using an Octet Red96 instrument
396 (FortéBio). Briefly, anti-human Fab (CH1-specific) sensors were used to capture sotrovimab and VIR-
397 7832 at 10 µg/ml for 10 minutes. The IgG-loaded sensors were then exposed to kinetics buffer containing
398 3 µg/ml of purified human C1q for 4 minutes, followed by a dissociation step in the same buffer for
399 additional 4 minutes. Association and dissociation profiles were measured in real time as changes in the
400 interference pattern.

401 **Binding to Cell Surface Expressed SARS-CoV-2 Spike Protein.** The SARS-CoV-2 spike protein
402 coding sequence (YP_009724390.1, Wuhan-Hu-1 strain) was cloned into a cell expression plasmid under
403 the control of the human CMV promoter (phCMV1) to generate phCMV1 WT spike. ExpiCHO-S cells
404 were seeded the day before transfection at 3 x 10^6 cells/mL in ExpiCHO Expression Medium.
405 Immediately before transfection, the cells were seeded at 6 x 10^6 cells cells/mL in a volume of 15 mL in
406 125 mL shake flasks. Six µg of phCMV1 WT spike plasmid or vector control were diluted in 1.2 mL of
407 iced OptiPRO SFM., followed by addition of 48 µL of ExpiFectamine CHO Reagent and complexing for
408 1 minute at RT. The transfection mixture was added dropwise to cells with gentle swirling. Cells were
409 then incubated at 37°C, 8% CO2 with shaking for 42 hours. At 42 hours post-transfection, ExpiCHO-S
410 cells were harvested, washed twice with FACS buffer and resuspended at a concentration of 1.0 x 10^6
411 cell/mL in PBS. Cells (5 x 10^4 cells in 50 µl/wells) were dispensed into a 96-well V-bottom plate.
412 Antibody was serially diluted (1:4, 10 points) starting at a concentration of 10 µg/mL. Cells were pelleted
413 at 300 x g for 5 minutes and resuspended in 50 µL/well of antibody serial dilutions and plates were
414 incubated for 45 mins on ice. Cells were washed twice in FACS buffer. Alexa Fluor 647-labelled Goat
415 Anti-Human IgG secondary Ab was diluted 1:750 in FACS buffer and 50 µL was added to the cell pellet

416 for 15 min on ice. Cells were washed twice with FACS buffer, resuspended in 1% PFA. Data was
417 acquired by flow cytometry (CytoFlex LX).

418 **Pseudotyped virus production.** Lenti-X™ 293T cells were seeded in 10-cm dishes for 80% next day
419 confluency. The next day, cells were transfected with the plasmid pcDNA3.1(+)-spike-D19 (encoding the
420 SARS-CoV-2 spike protein) or pcDNA3.1(+)-spike-D19 variants using the transfection reagent TransIT-
421 Lenti according to the manufacturer's instructions. One day post-transfection, cells were infected with
422 VSV-luc (rVSVΔG; Kerafast) at an MOI of 3. The cell supernatant containing SARS-CoV-2 pseudotyped
423 virus was collected at day 2 post-transfection, centrifuged at 1000 x g for 5 minutes to remove cellular
424 debris, aliquoted and frozen at -80°C.

425 **In Vitro Neutralization of SARS-CoV-2 Pseudotyped Virus.** VeroE6 cells were seeded into flat
426 bottom tissue culture 96-well plates at 20,000 cells/well and cultured overnight at 37°C. Twenty-four
427 hours later, 9-point 1:4 serial dilutions of VIR-7831 were prepared in infection medium and each dilution
428 was tested in triplicate per plate (range: 20,000 to 0.3 ng/mL final concentration). SARS-CoV-2 virus
429 stock was diluted in infection media for a final concentration of 2000 plaque forming units per well (MOI
430 0.1). Antibody dilutions were added to virus and incubated for 30 minutes at 37°C. Media was removed
431 from the VeroE6 cells, mAb-virus complexes were added, and cells were incubated at 37°C. At 6 hours
432 post-infection, cells were fixed with 250 µL 4% PFA, incubated for 30 minutes at RT, then washed 3
433 times with PBS to remove residual PFA. The cells were permeabilized with 50 µL of 0.125% Triton X-
434 100 in PBS for 30 minutes at RT. The blocking buffer was removed, 50 µL of SARS-CoV-2 nucleocapsid
435 antibody at 1:2,000 in blocking buffer was added, and plate was incubated for 1 hour at RT. Plates were
436 washed three times with PBS and then incubated for 1 hour at RT with 50 µL/well of goat anti-rabbit-
437 Alexa647 secondary antibody at a final dilution of 1:1,000 mixed with 2 ug/mL Hoechst dye in blocking
438 buffer. After washing 5 times with PBS, 100 µL of fresh PBS was added for imaging. Plates were imaged
439 on a Cytation5 plate reader. Whole well images were acquired (12 images at 4X magnification per well)
440 and nucleocapsid-positive cells were counted using the manufacturer's software.

441 **Live virus neutralization.** VeroE6 cells were seeded into flat bottom tissue culture 96-well plates at
442 20,000 cells/well and cultured overnight at 37°C. Twenty-four hours later, 9-point 1:4 serial dilutions of
443 VIR-7831 were prepared in infection medium and each dilution was tested in triplicate per plate (range:
444 20,000 to 0.3 ng/mL final concentration). SARS-CoV-2 virus stock was diluted in infection media for a
445 final concentration of 2000 plaque forming units per well (MOI 0.1). Antibody dilutions were added to
446 virus and incubated for 30 minutes at 37°C. Media was removed from the VeroE6 cells, mAb-virus
447 complexes were added, and cells were incubated at 37°C. At 6 hours post-infection, cells were fixed with
448 250 µL 4% PFA, incubated for 30 minutes at RT, then washed 3 times with PBS to remove residual PFA.
449 The cells were permeabilized with 50 µL of 0.125% Triton X-100 in PBS for 30 minutes at RT. The
450 blocking buffer was removed, 50 µL of SARS-CoV-2 nucleocapsid antibody at 1:2,000 in blocking buffer
451 was added, and plate was incubated for 1 hour at RT. Plates were washed three times with PBS and then
452 incubated for 1 hour at RT with 50 µL/well of goat anti-rabbit-Alexa647 secondary antibody at a final
453 dilution of 1:1,000 mixed with 2 ug/mL Hoechst dye in blocking buffer. After washing 5 times with PBS,
454 100 µL of fresh PBS was added for imaging. Plates were imaged on a Cytation5 plate reader. Whole well
455 images were acquired (12 images at 4X magnification per well) and nucleocapsid-positive cells were
456 counted using the manufacturer's software..

457 **Determination of Viral Titer by Focus-Forming Assay.** One day prior to infection, $1.2X10^4$ VeroE6
458 cells were plated in black-walled, clear bottomed 96-well plates. Virus samples were diluted 1:5 in
459 infection media and adsorbed onto VeroE6 cells for one hour at 37°C. The cells were washed once and
460 overlaid with 1% methylcellulose/serum-containing media. At 24 hours post-infection, the
461 methylcellulose overlay was removed, and cells were washed with PBS. Cells were fixed with 4% PFA,
462 incubated for 30 minutes at RT, then washed with PBS to remove residual PFA. The cells were
463 permeabilized with 50 µL of 0.25% Triton X-100 in PBS for 30 minutes at RT. The Triton X-100 was
464 removed, cells were washed twice with PBS, and incubated with 50 µL of SARS-CoV-2 nucleocapsid
465 antibody at 1:2,000 in blocking buffer for one hour at RT. Plates were washed three times with PBS and

466 then incubated for one hour at RT with 50 µL/well of goat anti-rabbit-Alexa647 secondary antibody at
467 1:1,000 in blocking buffer. After washing three times with PBS, 50 µL of Hoechst dye at 1:1,000 in PBS
468 was added for imaging. Plates were imaged on a Cytation5 plate reader. Whole well images were
469 acquired (12 images at 4X magnification per well) and nucleocapsid-positive foci were counted using the
470 manufacturer's software and used to determine focus-forming units/mL supernatant (FFU/mL).

471 **Determination of mAb-Dependent Activation of Human FcγRIIa, FcγRIIIa or FcγRIIb.** Sotrovimab,
472 VIR-7832, S309-LS, and a control mAb with abrogated FcγR binding, S309-GRLR, were serially diluted
473 6-fold in assay buffer from 10,000 ng/ml to 0.006 ng/ml. Nine-point serial dilutions of mAbs were
474 incubated with 12,500 (for FcγRIIIa and FcγRIIb) or 10,000 (for FcγRIIa) CHO-CoV-2-Spike cells per
475 96-plate well in a white, flat-bottom plate for 15 minutes at room temperature. Jurkat effector cells
476 expressing indicated FcγRs and stably transfected with an NFAT-driven luciferase gene were thawed,
477 diluted in assay buffer, and added to the plate at an effector to target cell ratio of 6:1 for FcRγIIIa and
478 FcγRIIb or 5:1 for FcγIIa. Control wells were also included that were used to measure antibody-
479 independent activation (containing target cells and effector cells but no antibody) and background
480 luminescence of the plate (wells containing assay buffer only). Plates were incubated for 18 hours at 37°C
481 with 5% CO2. Activation of human FcγRs in this bioassay results in the NFAT-mediated expression of
482 the luciferase reporter gene. Luminescence was measured with a luminometer after adding the Bio
483 GloTM Luciferase Assay Reagent according to the manufacturer's instructions. To control for
484 background, the mean of the relative luminescence units (RLU) values in wells containing only Assay
485 Buffer was calculated and subtracted from all data points. Data were expressed as the average of RLUs
486 over the background

487 **Determination of NK-Cell Mediated Antibody-Dependent Cellular Cytotoxicity.** Primary NK cell
488 activation was tested using freshly isolated cells from two previously genotyped donors expressing
489 homozygous low affinity (F158) or high affinity (V158) FcγRIIIa. Serial dilutions of mAbs (serially
490 diluted 10-fold in AIM-V Medium from 40,000 ng/ml to 0.075 ng/ml) were incubated with 7,500 CHO-

491 CoV-2 Spike cells per well of a 96 well round-bottom plate for 10 minutes. Target cell and antibody
492 mixtures were then incubated with primary human NK cells as effectors at an effector-to-target ratio of
493 10:1. ADCC was measured using lactate dehydrogenase (LDH) release as a readout according to the
494 manufacturer's instructions (Cytotoxicity Detection Kit (LDH), Roche) after 4 hours of incubation at
495 37°C. In brief, plates were centrifuged for 4 minutes at 400 x g, and 35 µl of supernatant was transferred
496 to a flat 384 well plate. LDH reagent was prepared and 35 µl were added to each well. Using a kinetic
497 protocol, the absorbance at 490 nm and 650 nm was measured once every 2 minutes for 8 minutes, and
498 the slope of the kinetics curve was used as result. The percent specific lysis was determined by applying
499 the following formula: (specific release – spontaneous release) / (maximum release - spontaneous release)
500 x 100.

501 **Determination of Monocyte-Mediated Antibody-Dependent Cellular Phagocytosis.** ADCP assays
502 were performed using human PBMCs freshly isolated from whole blood. CHO CoV-2-Spike cells were
503 used as target cells and were fluorescently labeled with PKH67 Fluorescent Cell Linker Kit (Sigma
504 Aldrich) prior to incubation with mAbs, according to manufacturer's instructions. Serial dilutions of
505 mAbs (serially diluted 5-fold from 5,000 ng/ml to 0.32 ng/ml in RPMI-1640 + L-glutamine supplemented
506 with 10% Hyclone FBS + 2x anti-anti (antibiotic-antimycotic)) were incubated with 10,000 CHO-CoV-2-
507 Spike cells per well of a 96 well polypropylene plate for 10 minutes. Primary PBMCs were fluorescently
508 labeled with Cell Trace Violet according to the manufacturer's instructions. Target cell and antibody
509 mixtures were then incubated with labeled PBMCs at an effector-to-target ratio of 16:1. After an
510 overnight incubation at 37°C, monocytes were stained with anti-human CD14-APC antibody (BD
511 Pharmingen). Antibody-mediated phagocytosis was determined by flow cytometry, gating on CD14+
512 cells that were double positive for cell trace violet and PKH67. Raw data were exported from the flow
513 cytometer into the flow cytometry analysis software FlowJo v10 (Becton Dickinson) for gating and
514 determination of the percentage of $CD14^+$ cells that were also double positive for cell trace violet and
515 PKH67. Cells expressing only cell trace violet or only PKH67 were used to set the positive staining gates.

516 **In vitro resistance selection.** The selection of variants in the presence of increasing concentrations of
517 VIR-7832 was conducted in VeroE6 cells. The day before infection, 6 x 10^4 VeroE6 cells were seeded in
518 24 well plates and incubated overnight at 37°C. The next day, 600 focus forming units (FFU) of SARS-
519 CoV-2 virus (MOI = 0.01) was incubated with 0.5X IC_{50} of VIR-7832 (0.05 µg/mL) at 37°C for one hour
520 in infection media. The mAb-virus complexes were adsorbed on VeroE6 cells for one hour at 37°C in
521 duplicate wells. After adsorption, cells were washed with DMEM and overlaid with infection media
522 containing 0.05 µg/mL VIR-7832. Control wells infected without antibody were included with each
523 passage. Infected cells were monitored visually for CPE daily. In general, when infected cells exhibited ≥
524 50% CPE, the culture supernatants were harvested, diluted 1:200, and added to fresh VeroE6 cells in 24-
525 well plates with equivalent or increasing concentrations of VIR-7832. At each passage, supernatant was
526 aliquoted and frozen at -80°C for titer and neutralization analyses.

527 **In vitro assessment of potential for ADE.** VeroE6 cells were plated at 1.25X10^4 cells/well one day prior
528 to infection. For each independent experiment, moDCs and PBMCs from five unique moDC donors and
529 six unique PBMC donors were used, with three unique donors used for each independent experiment.
530 Cryopreserved monocytes from unique donors were differentiated into moDCs for six days using human
531 moDC differentiation media according to the manufacturer's protocol. Cryopreserved PBMCs from
532 unique donors are thawed in the presence 0.3 mg/mL DNase and cultured in media for one day prior to
533 infection. On the day of infection, moDCs, PBMCs, and U937 cells were counted and plated at 7.5X10^4
534 cells/well.

535 To examine viral entry, 24 hours post-infection, cells were fixed with 4% PFA, incubated for 30 minutes
536 at RT, then washed with PBS to remove residual PFA. The cells were permeabilized with 50 µL of 0.25%
537 Triton X-100 in PBS for 30 minutes at RT. The Triton X-100 was removed, cells were washed twice with
538 PBS, and incubated with 50 µL of SARS-CoV-2 nucleocapsid antibody at 1:2,000 in blocking buffer for
539 one hour at RT. Plates were washed three times with PBS and then incubated for one hour at RT with 50
540 µL/well of goat anti-rabbit-Alexa647 secondary antibody at 1:1,000 in blocking buffer. After washing

541 three times with PBS, 50 µL of Hoechst dye at 1:1,000 in PBS was added for imaging. Plates were
542 imaged on a Cytation5 plate reader. Whole well images were acquired (12 images at 4X magnification
543 per well) and nucleocapsid-positive cells were counted using the manufacturer's software. The percent of
544 nucleocapsid+ cells was quantified using the Gen5 Imager software (Biotek, Vermont) as number of
545 Cy5+ cells, [(nucleocapsid+ cells)/number of Hoechst+ cells (total cells)]x100. Data was analyzed using
546 Prism v8.00 (GraphPad Software, La Jolla California USA, www.graphpad.com).

547 In order to quantify chemokines and cytokines from supernatants in a BSL2 laboratory, supernatants were
548 inactivated by 10 minutes exposure to UVC light at 5,000 µJ/cm2. Supernatants were diluted 1:5 in
549 infection media and levels of cytokines/chemokines were quantified using the U-plex 96-well assay
550 according to the manufacturer's protocol (Meso Scale Diagnostics, Rockville, MD). Quantification of
551 cytokines and chemokines were determined based on an 8-point standard curve in duplicate, provided by
552 the manufacturer. Cytokine data was analyzed using the Discovery Workbench v4.0.13 software (Meso
553 Scale Diagnostics). Data was graphed and statistical analyses were conducted using Prism software.

554 **Sequencing of SARS-CoV-2 Spike Gene.** To isolate nucleic acid from the supernatant of viral passages,
555 120 µL of cell supernatant was added to 360 µL of Trizol and stored at -80°C for further analysis. Trizol
556 collected samples from viral passages where a shift in neutralization > 2-fold relative to wild type was
557 detected were subjected to RNA isolation using PureLink RNA Mini Kit with the incorporation of on-
558 column PureLink DNase Treatment, following manufacturer's instructions. Reverse transcription
559 reactions were performed with 6 µL of purified RNA and oligoT primers using the NEB ProtoScript II
560 First Strand cDNA Synthesis kit, according to manufacturer's instructions. The resulting cDNA was used
561 as a template for PCR amplification of the spike gene using the KapaBiosystems polymerase (KAPA HiFi
562 HotStart ReadyMix) with primers 5' aattatcttggcaaaccacg-3' and 5' tgaggcttgtatcggtatcg-3'.
563 Amplification conditions included an initial 3 minutes at 95°C, followed by 28 cycles with 20 seconds at
564 98°C, 15 seconds at 62°C and 72°C for 2 minutes, with a final 4 minutes at 72°C. PCR products were
565 purified using AMPure XP beads following manufacturer's instructions. The size of the amplicon was

566 confirmed by analyzing 2 μL of PCR products using the Agilent D5000 ScreenTape System. Products
567 were quantified by analyzing 1 μL with the Quant-iT dsDNA High-Sensitivity Assay Kit. Twenty ng of
568 purified PCR product was used as input for library construction using the NEBNext Ultra II FS DNA
569 Library Prep kit following manufacturer's instructions. DNA fragmentation was performed for 13
570 minutes. NEBNext Multiplex Oligos for Illumina Dual Index Primer Set 1 was used for library
571 construction, with a total of 6 PCR cycles. Libraries size was determined using the Agilent D1000
572 ScreenTape System and quantified with the Quant iT dsDNA High-Sensitivity Assay Kit. Equal amounts
573 of each library were pooled together for multiplexing and 'Protocol A: Standard Normalization Method'
574 of the Illumina library preparation guide was used to prepare 8 pM final multiplexed libraries with 1%
575 PhiX spike-in for sequencing. The MiSeq Reagent Kit v3 (600-cycle) was used for sequencing the
576 libraries on the Illumina MiSeq platform, with 300 cycles for Read 1, 300 cycles for Read 2, 8 cycles for
577 Index 1, and 8 cycles for Index 2.

578 **Bioinformatics Analysis of Conservation.** Available genome sequences for SARS-CoV-2 were
579 downloaded from Global Initiative on Sharing All Influenza Data (GISAID; https://www.gisaid.org/) on
580 June 4, 2021. Bat and pangolin sequences were removed to yield human-only sequences. The spike open
581 reading frame was localized by aligning the reference protein sequence (NCBI reference sequence:
582 YP_009724390.1) to the genomic sequence of isolates with Exonerate v.2.4.0. Coding nucleotide
583 sequences were translated in silico using seqkit v.0.12.0. Multiple sequence alignment was performed
584 using MAFFT v.7.455. Variants were determined by comparison of aligned sequences to the reference
585 sequence using the R v3.6.3/Bioconductor v.3.10 package Biostrings v.2.54.0.

586 **In vivo studies.** Syrian golden hamster studies were conducted at Lovelace Biomedical (Albuquerque,
587 NM). Twelve- to sixteen-week-old male hamsters were interperitoneally administered a non-LS version
588 of VIR-7831 (SGHmAb-no-LS), control antibody or diluent Day -1 or Day -2 prior to virus challenge.
589 Animals were inoculated intranasally at Day 0 with 7.4×10^4 $TCID_{50}$ with SARS-CoV-2 (isolate USA-
590 WA1/2020). Animals were also weighed once daily in the morning beginning on study Day -10 and

591 continuing until the end of the study. Following euthanasia, RT-qPCR was performed on lung
592 homogenates using quantitative real-time PCR methods targeting the SARS-CoV-2 N gene and the
593 median tissue culture infections dose ($TCID_{50}$) was determined per Lovelace internal methodology.

594 **Author Contributions**

595 Conceived studies: A.L.C, C.H-D., F.A.P, D.M., M.S., L.S., A.T., L.A.P., S.H., G.S., H.W.V., D.C., C.M.H.
596 Designed studies and experiments: A.L.C, C.H.D., F.A.P, D.M., M.S., M.L.A., E. D., B.G., J.D., L.R.,A.C., A.S.,
597 R.S., J.W., N.C., E.C., S.L., C.C., D.P., C.S., J.N., A.P., A.W., L.S., A.T., L.A.P., S.H., G.S., H.W.V., D.C., C.M.H.
598 Performed experiments: D.M., M.S., M.L.A., B.G., J.D., E.D., A.S., L.R., H.T., J.D., S.S., D.P., C.S., J.N., B.S.,
599 S.B., J.W., J.Z., H.K., A.C., M.M-R., A.P., A.W., N.C., E.C. Analyzed and interpreted data: A.L.C., C.H-D.,
600 F.A.L., D.M., M.S., M.L.A., B.G., J.D., D.P., C.S., J.N., E.L., A.S., R.S., L.R., H.T., B.S., S.B., J.W., J.Z., H.K., A.C.,
601 M. M-R., N.C., E.C., S.L., A.W., C.C., L.S., A.T., S.H., G.S., H.W.G, D.C., C.M.H. Prepared the manuscript
602 with input from all authors: A.L.C., G.S., A.T., L.P., D.C., H.W.G., C.M.H.

603 **Competing interests**

604 Some authors are current or former employees of Vir Biotechnology or Humabs BioMed SA (a fully-
605 owned subsidiary of Vir Biotechnology) and may hold shares in Vir Biotechnology. H.W.V. is a founder of
606 PierianDx and Casma Therapeutics. This research was sponsored and funded by Vir Biotechnology in
607 collaboration with GSK.

608

609 **REFERENCES**

610

611 1. WHO Coronavirus Disease (COVID-19) Dashboard | WHO Coronavirus Disease (COVID-19)
612 Dashboard. https://covid19.who.int/.

613 2. Levin, A. T. *et al.* Assessing the age specificity of infection fatality rates for COVID-19:
614 systematic review, meta-analysis, and public policy implications. *Eur J Epidemiol* **35**, 1123–
615 1138 (2020).

616 3. Dennis, A. *et al.* Multi-organ impairment in low-risk individuals with long COVID.
617 doi:10.1101/2020.10.14.20212555.

618 4. Murphy, J. *et al.* Psychological characteristics associated with COVID-19 vaccine hesitancy
619 and resistance in Ireland and the United Kingdom. *Nat Commun* **12**, 29 (2021).

620 5. Khubchandani, J. *et al.* COVID-19 Vaccination Hesitancy in the United States: A Rapid
621 National Assessment. *J Commun Health* 1–8 (2021) doi:10.1007/s10900-020-00958-x.

622 6. Sallam, M. *et al.* High Rates of COVID-19 Vaccine Hesitancy and Its Association with
623 Conspiracy Beliefs: A Study in Jordan and Kuwait among Other Arab Countries. *Nato Adv Sci*
624 *Inst Se* **9**, 42 (2021).

625 7. Tegally, H. *et al.* Emergence and rapid spread of a new severe acute respiratory syndrome-
626 related coronavirus 2 (SARS-CoV-2) lineage with multiple spike mutations in South Africa.
627 *medRxiv* (2020) doi:10.1101/2020.12.21.20248640.

628 8. Naveca, F. *et al.* Phylogenetic relationship of SARS-CoV-2 sequences from Amazonas with
629 emerging Brazilian variants harboring mutations E484K and N501Y in the Spike protein -
630 SARS-CoV-2 coronavirus / nCoV-2019 Genomic Epidemiology - Virological.
631 https://virological.org/t/phylogenetic-relationship-of-sars-cov-2-sequences-from-amazonas-with-
632 emerging-brazilian-variants-harboring-mutations-e484k-and-n501y-in-the-spike-protein/585
633 (2011).

634 9. Rambaut, A. *et al.* Preliminary genomic characterisation of an emergent SARS-CoV-2 lineage
635 in the UK defined by a novel set of spike mutations - SARS-CoV-2 coronavirus / nCoV-2019
636 Genomic Epidemiology - Virological. https://virological.org/t/preliminary-genomic-
637 characterisation-of-an-emergent-sars-cov-2-lineage-in-the-uk-defined-by-a-novel-set-of-spike-
638 mutations/563 (2020).

639 10. Bamlanivimab EUA Letter of Authorization Reissue 02092021.
640 https://www.fda.gov/media/143603/download.

641 11. Casirivimab and Imdevimab EUA Fact Sheet for Healthcare Providers.
642 https://www.fda.gov/media/143892/download.

643 12. Lilly's neutralizing antibody bamlanivimab (LY-CoV555) prevented COVID-19 at nursing
644 homes in the BLAZE-2 trial, reducing risk by up to 80 percent for residents.
645 https://investor.lilly.com/node/44291/pdf.

646 13. Gottlieb, R. L. *et al.* Effect of Bamlanivimab as Monotherapy or in Combination With
647 Etesevimab on Viral Load in Patients With Mild to Moderate COVID-19. *Jama* **325**, 632–644
648 (2021).

649 14. VanBlargan, L. *et al.* An infectious SARS-CoV-2 B.1.1.529 Omicron virus escapes
650 neutralization by therapeutic monoclonal antibodies. *Res Square* (2021) doi:10.21203/rs.3.rs-
651 1175516/v1.

652 15. Cameroni, E. *et al.* Broadly neutralizing antibodies overcome SARS-CoV-2 Omicron
653 antigenic shift. *Nature* (2021) doi:10.1038/d41586-021-03825-4.

654 16. Liu, L. *et al.* Striking antibody evasion manifested by the Omicron variant of SARS-CoV-2.
655 *Nature* (2021) doi:10.1038/d41586-021-03826-3.

656 17. Schäfer, A. *et al.* Antibody potency, effector function, and combinations in protection and
657 therapy for SARS-CoV-2 infection in vivo. *J Exp Med* **218**, (2020).

658 18. Winkler, E. S. *et al.* Human neutralizing antibodies against SARS-CoV-2 require intact Fc
659 effector functions and monocytes for optimal therapeutic protection. *Biorxiv* 2020.12.28.424554
660 (2020) doi:10.1101/2020.12.28.424554.

661 19. Bournazos, S. & Ravetch, J. V. Fcγ Receptor Function and the Design of Vaccination
662 Strategies. *Immunity* **47**, 224–233 (2017).

663 20. Pinto, D. *et al.* Cross-neutralization of SARS-CoV-2 by a human monoclonal SARS-CoV
664 antibody. *Nature* **583**, 290–295 (2020).

665 21. Pinto, D. *et al.* Cross-neutralization of SARS-CoV-2 by a human monoclonal SARS-CoV
666 antibody. *Nature* **583**, 290–295 (2020).

667 22. Ko, S.-Y. *et al.* Enhanced neonatal Fc receptor function improves protection against primate
668 SHIV infection. *Nature* **514**, 642 (2014).

669 23. Zalevsky, J. *et al.* Enhanced antibody half-life improves in vivo activity. *Nat Biotechnol* **28**,
670 157 (2010).

671 24. Gaudinski, M. R. *et al.* Safety and pharmacokinetics of the Fc-modified HIV-1 human
672 monoclonal antibody VRC01LS: A Phase 1 open-label clinical trial in healthy adults. *Plos Med*
673 **15**, e1002493 (2018).

674 25. Bournazos, S., Corti, D., Virgin, H. W. & Ravetch, J. V. Fc-optimized antibodies elicit CD8
675 immunity to viral respiratory infection. *Nature* 1–9 (2020) doi:10.1038/s41586-020-2838-z.

676 26. Weitzenfeld, P., Bournazos, S. & Ravetch, J. V. Antibodies targeting sialyl Lewis A mediate
677 tumor clearance through distinct effector pathways. *J Clin Invest* **129**, 3952–3962 (2019).

678 27. Bournazos, S., Corti, D., Virgin, H. W. & Ravetch, J. V. Fc-optimized antibodies elicit CD8
679 immunity to viral respiratory infection. *Nature* 1–9 (2020) doi:10.1038/s41586-020-2838-z.

680 28. Diamond, M. *et al.* SARS-CoV-2 variants show resistance to neutralization by many
681 monoclonal and serum-derived polyclonal antibodies. *Res Square* (2021) doi:10.21203/rs.3.rs-
682 228079/v1.

683 29. Kallewaard, N. L. *et al.* Structure and Function Analysis of an Antibody Recognizing All
684 Influenza A Subtypes. *Cell* **166**, 596–608 (2016).

685 30. DiLillo, D. J., Tan, G. S., Palese, P. & Ravetch, J. V. Broadly neutralizing hemagglutinin
686 stalk–specific antibodies require FcγR interactions for protection against influenza virus in vivo.
687 *Nat Med* **20**, 143–151 (2014).

688 31. Dunand, C. J. H. *et al.* Both Neutralizing and Non-Neutralizing Human H7N9 Influenza
689 Vaccine-Induced Monoclonal Antibodies Confer Protection. *Cell Host Microbe* **19**, 800–813
690 (2016).

691 32. Leon, P. E. *et al.* Optimal activation of Fc-mediated effector functions by influenza virus
692 hemagglutinin antibodies requires two points of contact. *Proc National Acad Sci* **113**, E5944–
693 E5951 (2016).

694 33. Bruhns, P. *et al.* Specificity and affinity of human Fcγ receptors and their polymorphic
695 variants for human IgG subclasses. *Blood* **113**, 3716–3725 (2009).

696 34. Weitzenfeld, P., Bournazos, S. & Ravetch, J. V. Antibodies targeting sialyl Lewis A mediate
697 tumor clearance through distinct effector pathways. *J Clin Invest* **129**, 3952–3962 (2019).

698 35. Cheng, Z. J. *et al.* Development of a robust reporter-based ADCC assay with frozen, thaw-
699 and-use cells to measure Fc effector function of therapeutic antibodies. *J Immunol Methods* **414**,
700 69–81 (2014).

701 36. Arvin, A. M. *et al.* A perspective on potential antibody-dependent enhancement of SARS-
702 CoV-2. *Nature* 1–11 (2020) doi:10.1038/s41586-020-2538-8.

703 37. Joyner, M. J. & Wright, R. S. Safety Update: COVID-19 Convalescent Plasma in 20,000
704 Hospitalized Patients. *Mayo Clinic Proceedings* (2020).

705 38. Weinreich, D. M. *et al.* REGN-COV2, a Neutralizing Antibody Cocktail, in Outpatients with
706 Covid-19. *New Engl J Med* **384**, 238–251 (2020).

707 39. Arvin, A. M. *et al.* A perspective on potential antibody-dependent enhancement of SARS-
708 CoV-2. *Nature* **584**, 353–363 (2020).

709 40. Khurana, S. *et al.* Vaccine-induced anti-HA2 antibodies promote virus fusion and enhance
710 influenza virus respiratory disease. *Sci Transl Med* **5**, 200ra114 (2013).

711 41. Winarski, K. L. *et al.* Antibody-dependent enhancement of influenza disease promoted by
712 increase in hemagglutinin stem flexibility and virus fusion kinetics. *Proc National Acad Sci* **116**,
713 15194–15199 (2019).

714 42. Hui, K. P. Y. *et al.* Tropism, replication competence, and innate immune responses of the
715 coronavirus SARS-CoV-2 in human respiratory tract and conjunctiva: an analysis in ex-vivo and
716 in-vitro cultures. *Lancet Respir Medicine* (2020) doi:10.1016/s2213-2600(20)30193-4.

717 43. Liu, Z. *et al.* Identification of Common Deletions in the Spike Protein of Severe Acute
718 Respiratory Syndrome Coronavirus 2. *J Virol* **94**, (2020).

719 44. Baum, A. *et al.* Antibody cocktail to SARS-CoV-2 spike protein prevents rapid mutational
720 escape seen with individual antibodies. *Science* **369**, 1014–1018 (2020).

721 45. Thomson, E. C. *et al.* Circulating SARS-CoV-2 spike N439K variants maintain fitness while
722 evading antibody-mediated immunity. *Cell* (2021) doi:10.1016/j.cell.2021.01.037.

723 46. Starr, T. N., Greaney, A. J., Dingens, A. S. & Bloom, J. D. Complete map of SARS-CoV-2
724 RBD mutations that escape the monoclonal antibody LY-CoV555 and its cocktail with LY-
725 CoV016. doi:10.1101/2021.02.17.431683.

726 47. Wise, J. Covid-19: The E484K mutation and the risks it poses. *Bmj* **372**, n359 (2021).

727 48. Chen, R. E. *et al.* Resistance of SARS-CoV-2 variants to neutralization by monoclonal and
728 serum-derived polyclonal antibodies. *Nat Med* 1–10 (2021) doi:10.1038/s41591-021-01294-w.

729 49. Wang, P. *et al.* Increased Resistance of SARS-CoV-2 Variants B.1.351 and B.1.1.7 to
730 Antibody Neutralization. *Biorxiv* 2021.01.25.428137 (2021) doi:10.1101/2021.01.25.428137.

731 50. VIR-7831 for the Early Treatment of COVID-19 in Outpatients - Full Text View -
732 ClinicalTrials.gov. https://clinicaltrials.gov/ct2/show/NCT04545060?term=VIR-
733 7831&draw=2&rank=2.

734 51. A Study of Immune System Proteins in Participants With Mild to Moderate COVID-19
735 Illness - Full Text View - ClinicalTrials.gov.
736 https://clinicaltrials.gov/ct2/show/NCT04634409?term=VIR-7831&draw=2&rank=3.

737 52. Vir Biotechnology and GSK announce NHS-supported AGILE study to evaluate VIR-7832
738 in the early treatment of COVID-19 | GSK. https://www.gsk.com/en-gb/media/press-releases/vir-
739 biotechnology-and-gsk-announce-nhs-supported-agile-study-to-evaluate-vir-7832-in-the-early-
740 treatment-of-covid-19/.

741 53. CoVariants. https://covariants.org/.

742 54. Piccoli, L. *et al.* Mapping neutralizing and immunodominant sites on the SARS-CoV-2 spike
743 receptor-binding domain by structure-guided high-resolution serology. *Cell* (2020)
744 doi:10.1016/j.cell.2020.09.037.

745 55. Rappazzo, C. G. *et al.* Broad and potent activity against SARS-like viruses by an engineered
746 human monoclonal antibody. *Science* **371**, 823–829 (2021).

747 56. Sette, A. & Crotty, S. Adaptive immunity to SARS-CoV-2 and COVID-19. *Cell* **184**, 861–
748 880 (2021).

749 57. Stettler, K. *et al.* Specificity, cross-reactivity and function of antibodies elicited by Zika virus
750 infection. *Science* **353**, aaf8505 (2016).

751

752 **FIGURE LEGENDS**

753 **Figure 1.** Sotrovimab (VIR-7831) and VIR-7831 bind S and neutralize SARS-CoV-2 virus and S variants
754 in vitro. a) Binding of sotrovimab (VIR-7831; black circles) and VIR-7832 (blue squares) to SARS-CoV-
755 2 RBD was tested by ELISA. Shown is the average of four replicates and SD derived from three
756 independent experiments. b) Association and dissociation profiles of sotrovimab (VIR-7831) to SARS-
757 CoV-2-RBD were measured using SPR. The double reference subtracted curves (shown for single
758 replicates) are plotted together with the curve fit in black (obscured by close overlay with the data).
759 Values are from two independent experiments. c) Binding of sotrovimab (VIR-7831; black circles) and
760 VIR-7832 (blue squares) to cell-surface S protein was determined by flow cytometry. Data are expressed
761 as the percentage of the positive cells. Results shown are from one experiment and representative of three
762 independent experiments performed. d) In vitro neutralization of live SARS-CoV-2 by different
763 concentrations of Sotrovimab (VIR-7831; left) and VIR-7832 (right) measured by nucleocapsid staining
764 6-hours post-infection. Results shown are from one experiment and representative of at least two
765 independent experiments performed. e) In vitro neutralization of Omicron BA.2 pseudotyped virus with
766 BA.1 and Alpha pseudotyped virus run as controls. Results shown are from one experiment and are
767 representative of ten independent experiments performed.

768 **Figure 2.** Sotrovimab (VIR-7831) and VIR-7832 demonstrate effector function in vitro. In vitro effector
769 function (a-e) activation profiles of human FcγRIIa (a), FcγRIIb (b), FcγRIIIa low-affinity (F158) (c) or
770 FcγRIIIa high-affinity binding allele (V158) (d) using bioreporter assays using S-expressing CHO cells as
771 the target antigen. Data points show means± SD of duplicates. NK-cell mediated killing (ADCC) of S-
772 expressing CHO cells using freshly isolated cells from two donors previously genotyped for homozygous
773 expression of low-affinity (F/F158) (e) or high-affinity (V/V158) FcγRIIIa (f). Data points are means of
774 quadruplicates ± SD. g) Antibody-dependent cellular phagocytosis (ADCP) using S-expressing CHO cells
775 and freshly isolated PBMCs. Data represent the means of duplicates ± SD.

776 **Figure 3.** Sotrovimab (VIR-7831) shows in vivo efficacy in a hamster SARS-CoV-2 model of infection.
777 a) Overview of hamster in vivo study design. b) and c) Animal weight over time as a percent of starting
778 weight in animals dosed a Day -1 (b) or Day -2 (c). Medians of at least N=6 animals and interquartile
779 range are shown. d) and e) Day 4 terminal weights expressed as a percentage of starting weight for
780 animals dosed at Day -1 (d) or Day -2 (e). Bar denotes median values. f) and g) Day 4 lung viral load in
781 Day -1 (f) or Day -2 (g) treated animals as assessed by RT-qPCR. Bar denotes median values. h) and i)
782 infectious virus in lung at Day 4 for Day -1 (h) or Day -2 (i) dosed animals. Bar denotes median values.
783 ns=not significant, ** = $p<0.05$, and *** = <0.005 as assessed by the Mann-Whitney U-test.

784 **Table 1.** Sotrovimab and VIR-7832 retain activity against S variants of concern in an authentic virus
785 system**.** Average fold change in sotrovimab and VIR-7832 IC_{50} compared to relative wild-type controls
786 for S variants tested in an authentic virus system. Data shown are averages of at least two independent
787 experiments.

788 **Table 2.** Sotrovimab and VIR-7832 retain activity against S variants of concern in a pseudotyped virus
789 system**.** Average fold change in sotrovimab and VIR-7832 IC_{50} compared to relative wild-type controls
790 for S variants tested in a VSV/VeroE6 pseudotyped virus system. Data shown are averages of at least two
791 independent experiments.

792 **Table 3.** Storovimab and VIR-7832 retain activity against variants that confer resistance to authorized or
793 approved mAbs. Activity of sotrovimab against variants conferring reduced susceptibility to
794 bamlanivimab, imdevimab or casirivimab in a VSV/VeroE6 pseudotyped virus system. The geometric
795 mean of IC_{50}s and average fold-change versus the relative wild-type control from at least two independent
796 experiments are shown.

797 **Table 4.** The sotrovimab/VIR-7832 epitope is highly conserved. Conservation data comprising
798 >4,500,000 sequences from the GISAID database and variants at each position are shown. Substitutions
799 in green were tested in a pseudotyped virus assay.

800

801 **Supplemental Figure 1.** Binding of sotrovimab (VIR-7831) and VIR-7832 to human FcγRs and C1q as
802 measured by SPR. Binding of sotrovimab (VIR-7831) and VIR-7832 to a) human FcγRIIa (H131 and
803 R131 alleles), FcγRIIIa (F158 and V158 alleles) and FcγRIIb were measured using SPR. Biotinylated
804 purified FcγRs were captured on the sensor chip surface prior to injection of sotrovimab (VIR-7831) or
805 VIR-7832. Association and dissociation profiles (separated by the vertical dotted line) were measured in
806 real time as change in the SPR signal. b) Binding of sotrovimab (VIR-7831) and VIR-7832 to
807 complement component C1q was measured using BLI on an Octet Red96 instrument. Association and
808 dissociation profiles (separated by the vertical dotted line) were measured in real time as change in the
809 interference pattern.

810 **Supplemental Figure 2.** Sub-neutralizing concentrations of sotrovimab (VIR-7831) and VIR-7832 do
811 not enhance viral entry, viral replication or cytokine production in vitro. Internalization (a) and replication
812 (b) of SARS-CoV-2 was evaluated in VeroE6, moDCs or PBMCs at various timepoints. Two independent
813 experiments with human moDCs and PBMCs from three individual donors were analyzed (5 unique
814 moDC donors, 6 unique PBMC donors total between two experiments). VeroE6 cells were run in
815 duplicate for both independent experiments. Data from each replicate well from two independent

816 experiments are plotted as individual points, with horizontal lines representing the median. Mann-
817 Whitney U-test comparison to no antibody group, *$p<0.05$. c) Supernatant cytokine and chemokine levels
818 as measured by MSD at the indicated time post infection. Data from two independent experiments (three
819 replicates each, five unique donors) are plotted as the mean and SD.

820 **Supplemental Figure 3.** Overview of VIR-7832 resistance selection method. All passaging was
821 conducted in duplicate wells. (a) VIR-7832 concentration was increased during each passage. P3 X
822 indicates passage 3 virus, after which virus was lost with subsequent increases in concentration. In (b) and
823 (c), p3X denotes where passage 3 virus from (a) was used to initiate (b) viral lineage 1 and (c) viral
824 lineage 2. Arrows indicate passages that were subjected to sequence analysis, and * indicate the passages
825 in lineage 1 with no detectable virus or CPE. Selection continued for a total of eight passages.

826 **Supplemental Table 1.** Amino acid substitutions identified in the SARS-CoV-2 S upon in vitro selection
827 with VIR-7832. Spike gene sequences were compared to a SARS-CoV-2 reference sequence (NCBI:
828 NC_045512.2) to identify variants. Fold-changes in IC_{50} were determined compared to the SARS-CoV-2
829 virus stock.

830 **Supplemental Table 2.** Sotrovimab and VIR-7832 activity against selected S variants. Sotrovimab/VIR-
831 7832 epitope variants observed by in vitro resistance selection were individually tested in a VSV/VeroE6
832 pseudotyped virus system. The geometric mean of IC_{50}s and average fold-change versus the relative wild-
833 type control from at least two independent experiments are shown.

834 **Supplemental Table 3.** Activity of sotrovimab against epitope variants. Sotrovimab/VIR-7832 epitope
835 variants detected in sequences from the GISAID database were tested in a VSV/VeroE6 pseudotyped
836 virus system. The geometric mean of IC_{50}s and average fold-change versus the relative wild-type control
837 from at least two independent experiments are shown.

838

Figure 1

a)

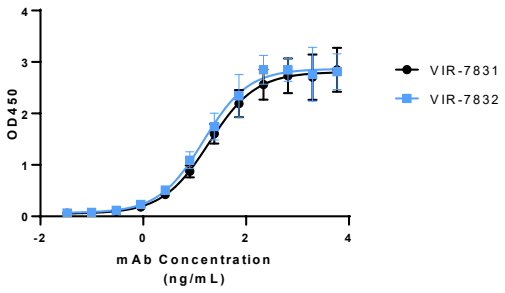

b)

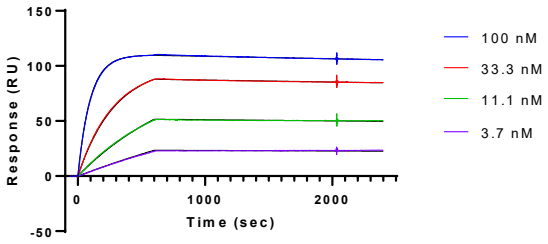

c)

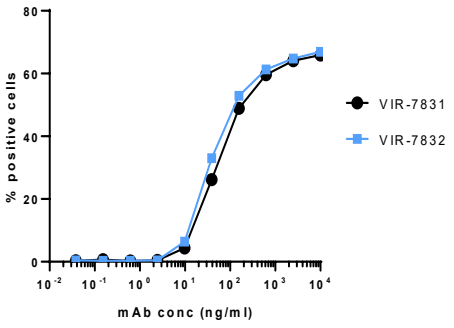

d)

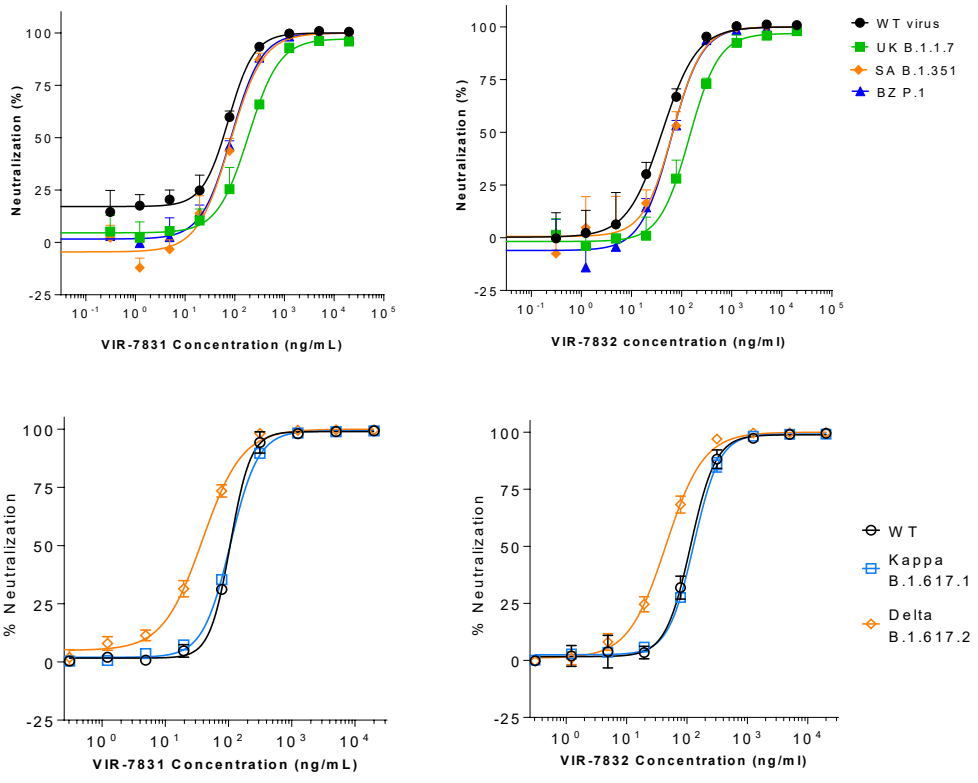

e)

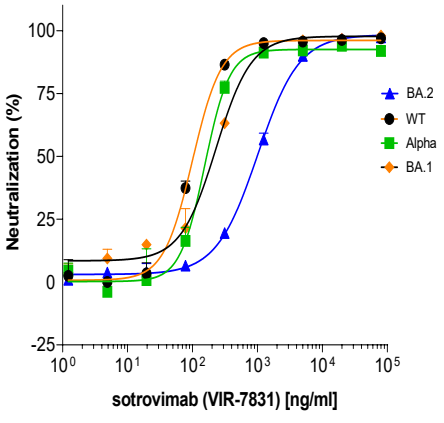

Figure 2

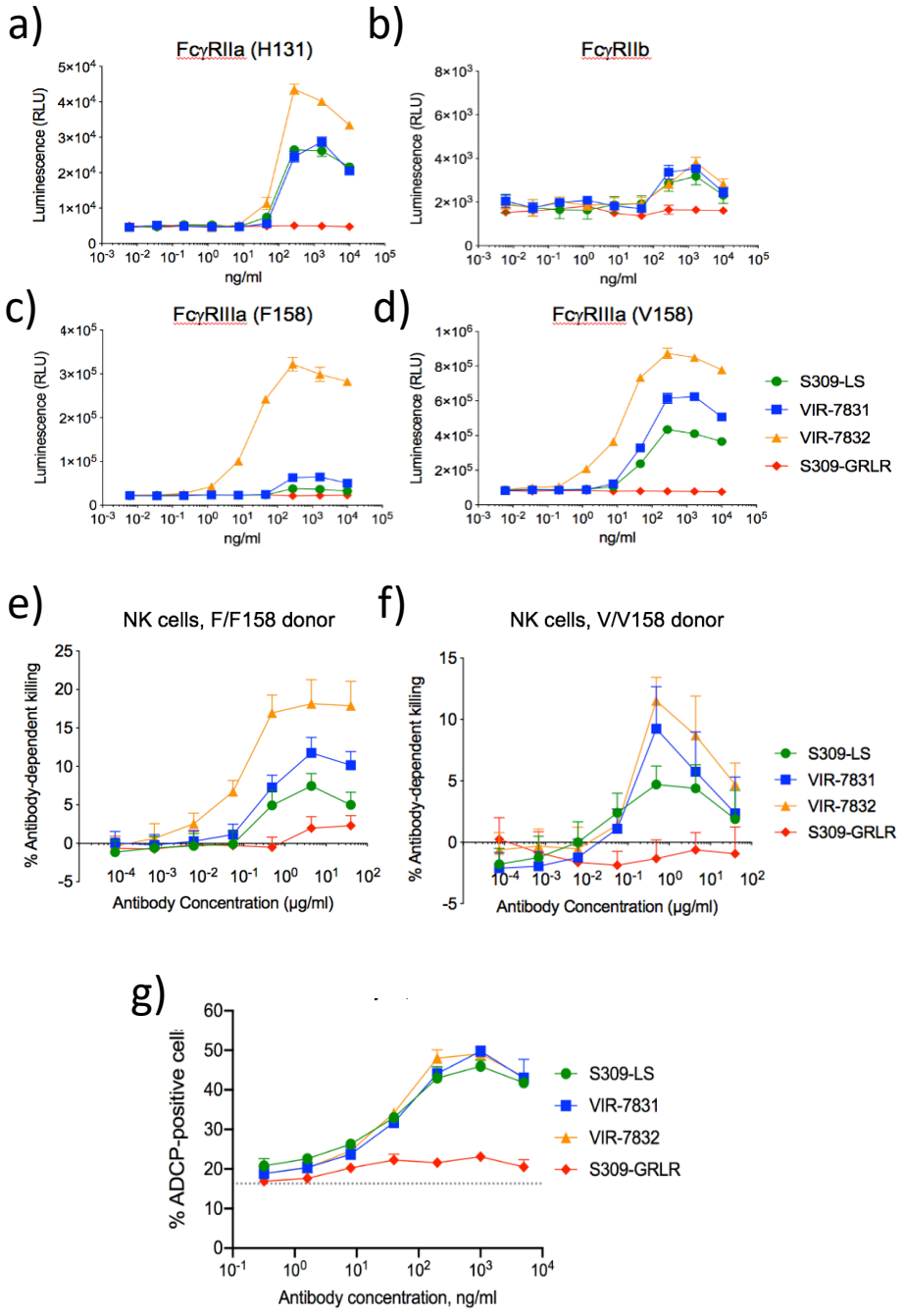
a)
FcγRIIa (H131)
Luminescence (RLU)
ng/ml
b)
FcγRIIb
Luminescence (RLU)
ng/ml
c)
FcγRIIIa (F158)
Luminescence (RLU)
ng/ml
d)
FcγRIIIa (V158)
Luminescence (RLU)
ng/ml
S309-LS
VIR-7831
VIR-7832
S309-GRLR
e)
NK cells, F/F158 donor
% Antibody-dependent killing
Antibody Concentration (μg/ml)
f)
NK cells, V/V158 donor
% Antibody-dependent killing
Antibody Concentration (μg/ml)
S309-LS
VIR-7831
VIR-7832
S309-GRLR
g)
% ADCP-positive cell
Antibody concentration, ng/ml
S309-LS
VIR-7831
VIR-7832
S309-GRLR

Figure 3

a)

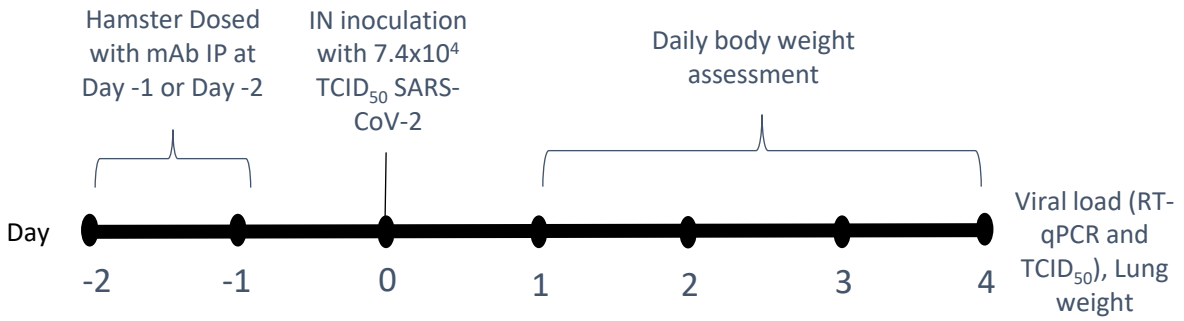

b)

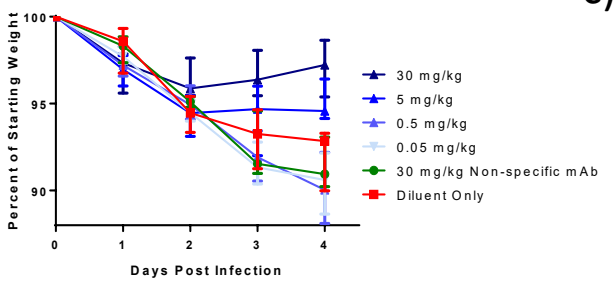

c)

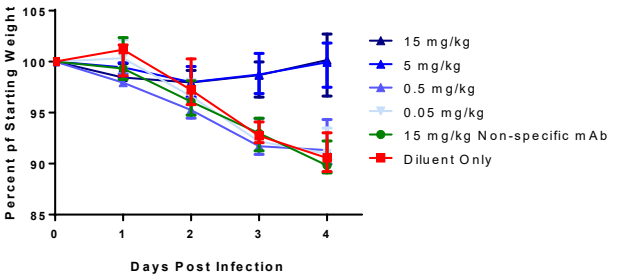

d)

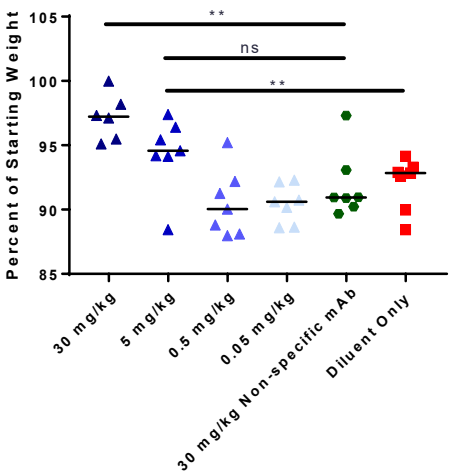

e)

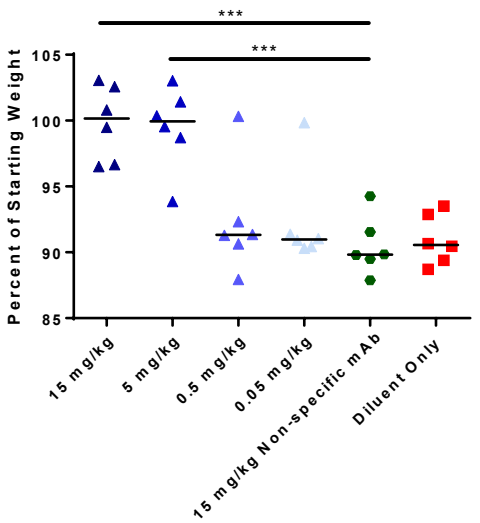

f)

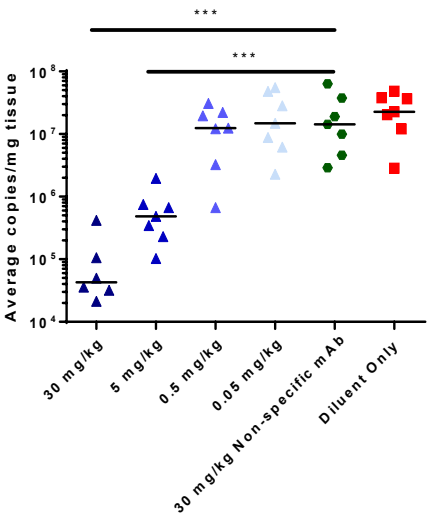

g)

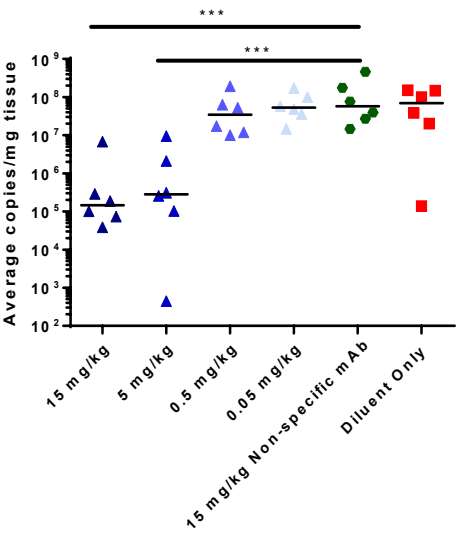

h)

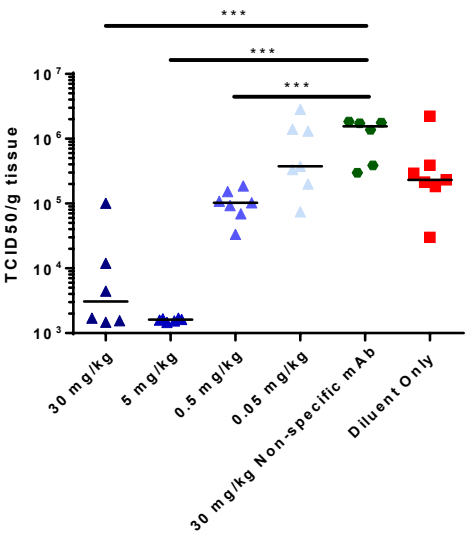

i)

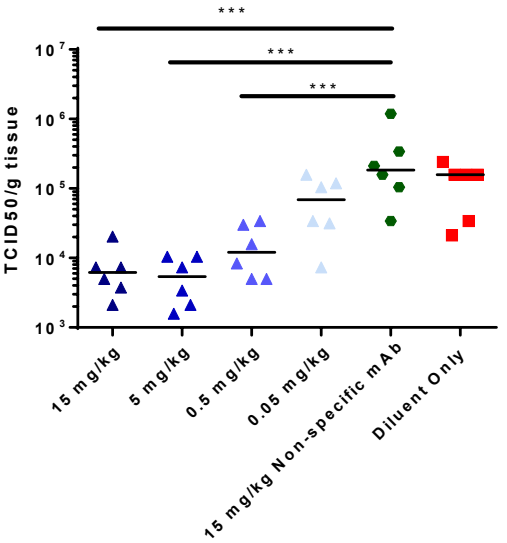

Table 1

SARS-CoV-2 Variant	**Geometric Mean Sotrovimab IC_{50} (ng/ml) (Average Fold Change IC_{50} vs. Wild-Type)**	**Geometric Mean Sotrovimab IC_{90} (ng/ml) (Average Fold Change IC_{90} vs. Wild-Type)**	**Geometric Mean VIR-7832 IC_{50} (ng/ml) (Average Fold Change IC_{50} vs. Wild-Type)**	**Geometric Mean VIR-7832 IC_{90} (ng/ml) (Average Fold Change IC_{90} vs. Wild-Type)**
Alpha (B.1.1.7)	187.15 (3.0)	1246.86 (4.1)	181.12 (3.1)	1222.95 (3.7)
Beta (B.1.351)	71.89 (1.2)	385.01 (1.3)	59.67 (1.1)	309.84 (0.9)
Gamma (P.1)	73.11 (1.6)	335.79 (1.4)	48.94 (1.2)	217.02 (0.9)
Delta (B.1.617.2)	51.29 (0.4)	219.08 (0.6)	59.13 (0.5)	274.24 (0.7)
Kappa (B.1.617.1)	118.64 (0.9)	379.89 (1.0)	132.37 (1.0)	428.83 (1.0)

Table 2

Variant	Spike Mutations	Fold-Change in Sotrovimab IC_{50} vs. Wild-type	Fold-Change in VIR-7832 IC_{50} vs. Wild-type
Alpha (B.1.1.7)	H69-, V70-, Y144-, N501Y, A570D, D614G, P681H, T716I, S982A, D1118H	2.3	2.5
Beta (B.1.351)	L18F, D80A, D215G, R246I, K417N, E484K, N501Y, D614G, A701V	0.6	0.7
Gamma (P.1)	D138Y, D614G, E484K, H655Y, K417T, L18F, N501Y, P26S, R190S, T1027I, T20N, V1176F	0.4	0.4
Delta (B.1.617.2)	T19R, G142D, E156G, F157-, R158-, L452R, T478K, D614G, P681R, D950N	1	NT
Epsilon (B.1.427/B.1.429)	S13I, W152C, L452R, D614G	0.7	NT
Eta (B.1.525)	Q52R, A67V, H69-, V70-, Y144-, E484K, D614G, Q677H, F888L	0.9	NT
Iota (B.1.526)	L5F, T95I, D253G, E484K, D614G, A701V	0.6	NT
Kappa (B.1.617.1)	T95I, G142D, E154K, L452R, E484Q, D614G, P681R, Q1071H	0.7	NT
Lambda (C.37)	G75V, T76I, del246-252, L452Q, F490S, T859N	1.5	NT
Mu (B.1.621)	T95I, Y144T, Y145S, ins146N, R346K, E484K, N501Y, D614G, P681H, D950N	1.3	NT
Omicron (BA.1)	A67V, H69del, V70del, T95I, G142D, V143del, Y144del, Y145del, N211del, L212I, ins214EPE, G339D, S371L, S373P, S375F, K417N, N440K, G446S, S477N, T478K, E484A, Q493R, G496S, Q498R, N501Y, Y505H, T547K, D614G, H655Y, N679K, P681H, N764K, D796Y, N856K, Q954H, N969K, L981F	2.7	NT
Omicron + R346K (BA.1.1)	A67V, H69del, V70del, T95I, G142D, V143del, Y144del, Y145del, N211del, L212I, ins214EPE, G339D, R346K, S371L, S373P, S375F, K417N, N440K, G446S, S477N, T478K, E484A, Q493R, G496S, Q498R, N501Y, Y505H, T547K, D614G, H655Y, N679K, P681H, N764K, D796Y, N856K, Q954H, N969K, L981F	3.3	NT
Omicron (BA.2)	T19I, del24-26, A27S, G142D, V213G, G339D, S371F, S373P, S375F, T376A, D405N, R408S, K417N, N440K, S477N, T478K, E484A, Q493R, Q498R, N501Y, Y505H, D614G, H655Y, N679K, P681H, N764K, D796Y, Q954H, N969K	16.0	NT
Delta Plus (AY.1)	T19R, T95I, G142D, E156G, F157-, R158-, W258L, K417N, L452R, T478K, D614G, P681R, D950N	1.1	NT
Delta Plus (AY.2)	T19R, V70F, G142D, E156G, F157-, R158-, A222V, K417N, L452R, T478K, D614G, P681R, D950N	1.3	NT
Delta Plus (AY. 4.2)	T19R, T95I, G142D, Y145H, E156G, F157, R158-, A222V, L452R, T478K, D614G, P681R, D950N	1.6	NT
Mexico/Swiss (B.1.1.519)	T478K, D614G, P681H, T732A	0.8	NT
Scotland (B.1.258)	H69-, V70-, N439K, D614G	0.9	NT
US (R.2)	E484K, D614G, Q677H, T732S, E1202Q	0.8	NT
Liverpool (A.23.1)	R102I, F157L, V367F, E484K, Q613H, P681R	1.1	NT
Cameroon (B.1.619)	I210T, N440K, E484K, D614G, D936N, S939F, T1027I	1.3	NT
Bristol (B.1.1.7+E484K)	H69-, V70-, Y144-, E484K, N501Y, A570D, D614G, P681H, T716I, S982A, D1118H	1.7	NT

Table 3

Amino Acid position	Substitution / Deletion	mAb with Reduced Susceptibility	Variants in Tested Spike Sequence	Sotrovimab IC_{50} (ng/ml)	Average Fold Change in IC_{50} Compared to Relative Wild-Type
E406	W	casirivimab+ imdevimab	E406W	53.66	0.74
K417	E	casirivimab	K417E	67.71	0.89
N439	K	imdevimab	N439K, D614G	17.05	0.86
N440	D	imdevimab	N440D	80.47	1.29
N440	K	imdevimab	N440K, D614G	19.99	0.48
K444	Q	imdevimab	K444Q	79.68	1.11
V445	A	imdevimab	V445A	41.74	3.38
G446	V/I	imdevimab	G446V, D614G	18.41	1.50
Y453	F	casirivimab	G261D, Y453F	27.28	2.19
L455	F	casirivimab	L455F, D614G	21.65	0.56
G476	S	casirivimab	G476S	36.97	2.94
E484	K	bamlanivimab	E484K, D614G	12.91	0.33
F486	V/I	casirivimab	F486V	82.24	1.10
Y489	H	casirivimab	Y489H	92.29	1.48
F490	S	bamlanivimab	F490S	33.10	0.85
Q493	K	casirivimab, bamlanivimab	Q483K	69.79	0.98
S494	P	casirivimab, bamlanivimab	S494P, D614G	29.10	2.50

Table 4

Amino Acid Position	Reference Amino Acid[a]	Substitutions Identified in order of Prevalence[b]	Percent Reference AA Conservation
332	I	V, T, N, D, S	>99.99
333	T	I, K, A, S, P, R	>99.99
334	N	K, Y, S, H, D, T, -, E, I	>99.99
335	L	F, V, S, -, G, M	>99.99
336	C	S*, -, P, R	>99.99
337	P	L, S, T, H, R, - , K	>99.99
339	G	D, S, C, V, F, -, N	99.98
340	E	D, K, A, G, Q, V, -, I	>99.99
341	V	I, F, A, -, G, L, P, S	>99.99
343	N	Y, -, D, K, S	>99.99
344	A	S, T, V, D, F, G, -, P	99.97
345	T	S, I, -, N	>99.99
346	R	K, S, I, G, T, -, F	99.66
354	N	K, D, S, T, H, Y, I, -, G, P	99.95
356	K	R, N, E, Q, M, T, -, G, W, Y, I, KR	99.98
357	R	K, I, -, T, G, S, C, L, RIS	99.95
358	I	V, L, F, -, T*, A, E*	>99.99
359	S	N, T, G, R, I, -, C, F	99.98
360	N	Y, S, -, K, D, F, T, A, L	>99.99
361	C	T*, -, G*, N*, F*, R*, S*, Y	>99.99
440	N	K, S, Y, T, D, I, E, -, F, H, R	99.79
441	L	R, F, I, P, V, -, Y, H, M, S, E, N	>99.99
509	R	-, K*, S*, T*, I*, H	>99.99

AA = amino acid

[a]NCBI reference sequence: YP_009724390.1

[b]Dash indicates a stop codon. Asterisks indicate the substitution could not be evaluated due to low expression of the spike protein containing this substitution

Supplemental Figure 1

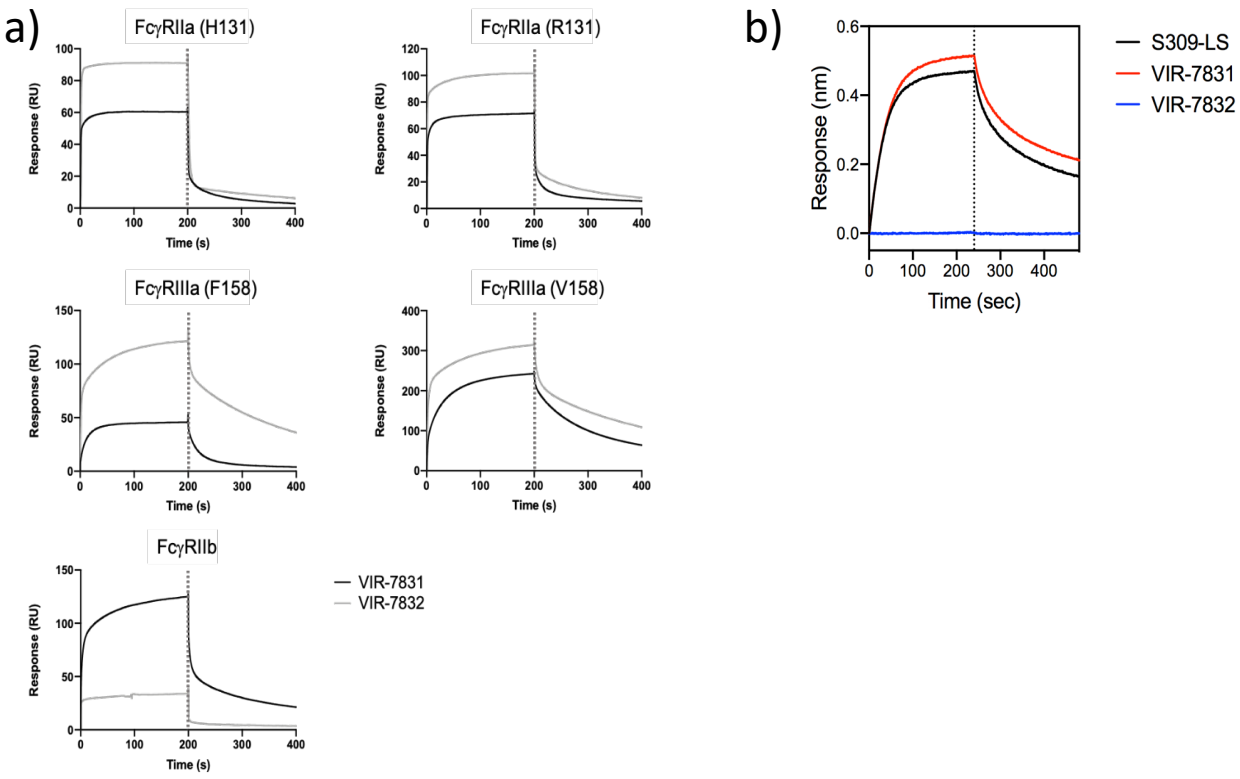

Supplemental Figure 2

a)

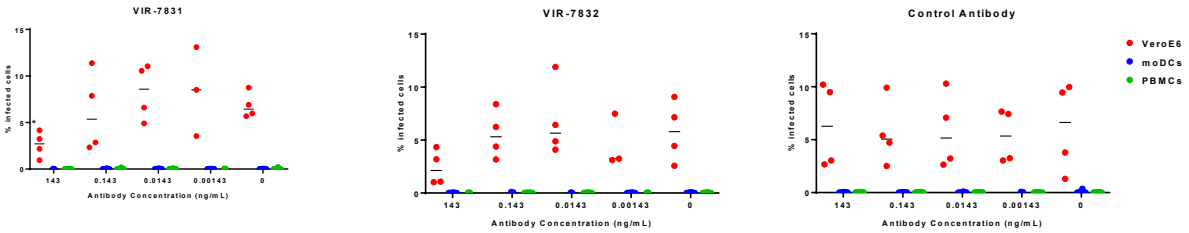

b)

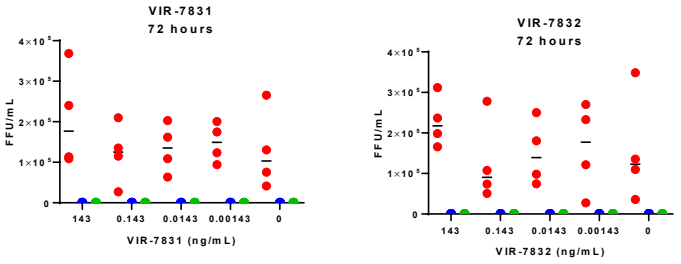

c)

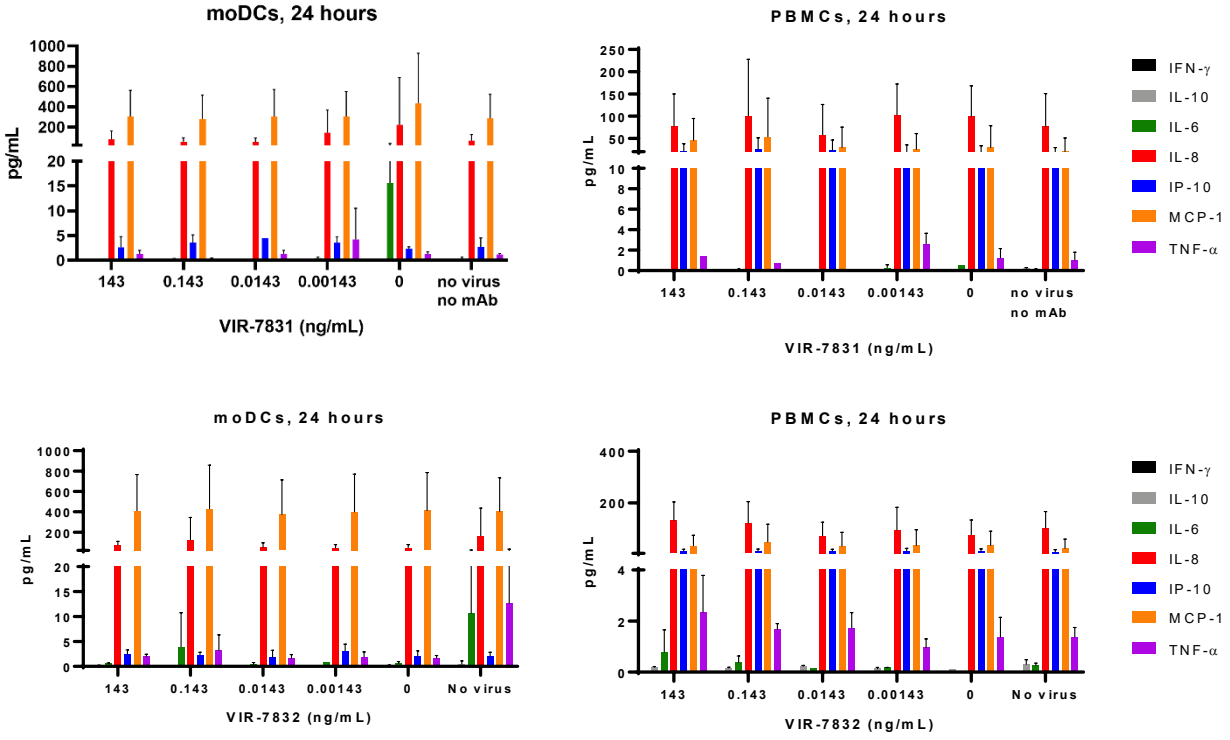

Supplemental Figure 3

a)

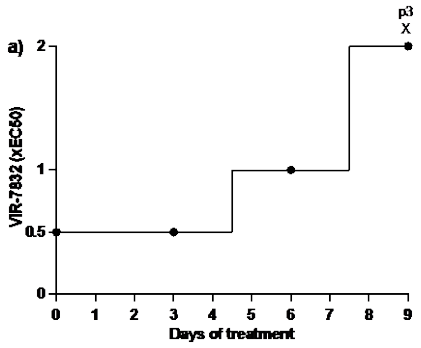

b)

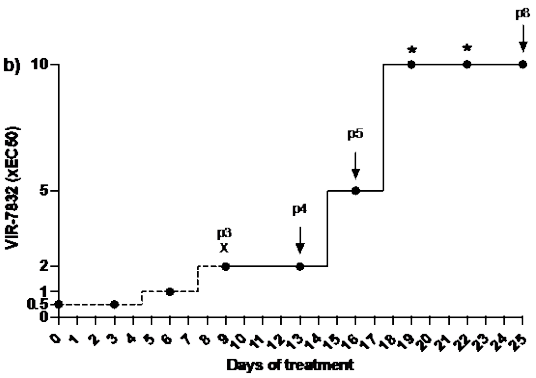

c)

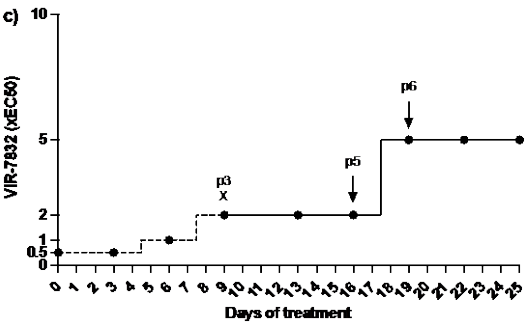

Supplemental Table 1

Passage	**Spike Gene Amino Acid Substitution (Freq)** [a,b]	**EC_{50} (µg/mL)**	**Fold Change in EC_{50} to WT**[c]
SARS-CoV-2 virus stock[c]	H66R (5.7%) N74K (12.6%) T76I (5.6%) 215-216insKLRS (60.9%) H655Y (3.1%)	0.06	NA
VIR-7832 Lineage 1, passage 4	215-216insKLRS (74.5%) 675-679 del (20.6%)	0.34	5.64
VIR-7832 Lineage 1, passage 5	215-216insKLRS (74.6%) 675-679del (66.0%)	0.35	5.93
VIR-7832 Lineage 1, passage 8	215-216insKLRS (74.7%) E340A (98.7%) 675-679del (84.5%)	ND	>10
VIR-7832 Lineage 2, passage 5	215-216insKLRS (73.9%) 675-679del (47.3%) R682W (4.9%) V1128F (3.5%)	0.32	5.40
VIR-7832 Lineage 2, passage 6	215-216insKLRS (75.3%) 675-679del (74.2%) R682W (4.9%) V1128F (30.9%)	0.39	6.54

Supplemental Table 2

Amino Acid Changes in Spike protein	Sotrovimab		VIR-7832	
	Geomean Neutralization IC_{50} (ng/mL)	**Fold Change Relative to Wild-Type**	**Geomean Neutralization IC_{50} (ng/mL)**	**Fold Change Relative to Wild-Type**
Wild Type[a]	104.46	NA	100.75	NA
E340A	> 10,000	>100	> 10,000	> 107
R682W	53.96	0.52	47.78	0.49
V1128F	50.65	0.53	49.69	0.60

Supplemental Table 3

Epitope Reference Amino Acid	Amino Acid Substitutions in Spike Protein	Geomean Neutralization IC_{50} (ng/mL)	Average Fold Change IC_{50} Relative to Reference[a]
I332	I332V, D614G	53.43	1.48
	I332T, D614G	66.74	1.61
T333	T333K, D614G	22.14	0.67
	T333I, D614G	30.93	0.59
N334	N334K, D614G	45.36	1.27
	N334H, D614G	30.74	0.87
	N334S, D614G	34.37	1.13
	N334Y, D614G	32.89	0.96
L335	L335F	29.19	0.81
	L335S, D614G	29.8	0.85
	L335V, D614G	42.2	0.63
P337	P337H, D614G	185.29	5.13
	P337L, D614G	>10000	>192
	P337K, D614G	>10000	>304
	P337R, D614G	>10000	>192
	P337S, D614G	127.69	1.26
	P337T, D614G	383.27	10.62
G339	G339D, D614G	117.38	1.18
	G339S, D614G	32.67	0.86
	G339C, D614G	68.79	1.18
	G339V, D614G	78.32	1.26
E340	E340A	>10000	>100
	E340D, D614G	81.46	2.45
	E340K	>10000	>297
	E340G, D614G	640.07	18.21
	E340Q, D614G	>2500	>50
	E340V, D614G	>10000	>200
V341	V341I, D614G	14.6	0.16
N343	N343S, D614G	16.87	0.48

Supplemental Table 3 (con't)

Epitope Reference Amino Acid	Amino Acid Substitutions in Spike Protein	Geomean Neutralization IC_{50} (ng/mL)	Average Fold Change IC_{50} Relative to Reference[a]
A344	A344S	92.19	0.89
	A344T, D614G	40.94	0.62
	A344V, D614G	53.87	1.14
	A344D, D614G	131.53	2.57
T345	T345S, D614G	42.92	0.69
	T345N, D614G	20.29	0.57
	T345I, D614G	11.78	0.20
R346	R346I, D614G	65.39	1.72
	R346S, D614G	42.87	1.13
	R346T, D614G	89.04	1.25
	R346K, D614G	24.76	0.72
	R346G, D614G	43.73	0.85
N354	N354D	104.8	1.00
	N354K, T95I	70.62	0.76
	N354H, D614G	74.88	1.06
	N354K, T95I	70.62	0.76
	N354S, D614G	61.78	0.89
	N354I, D614G	37.09	1.05
	N354T, D614G	43.32	0.65
	N354Y, D614G	67.63	1.08
K356	K356A	111.18	1.06
	K356R, D614G	29.61	0.78
	K356N, D614G	53.22	1.12
	K356M, D614G	64.09	1.03
	K356T, D614G	281.13	5.9
	K356E, D614G	76.54	1.65
	K356Q, D614G	43.2	0.94
R357	R357K, D614G	39.13	1.02
	R357I, D614G	46.41	0.98

Supplemental Table 3 (con't)

Epitope Reference Amino Acid	Amino Acid Substitutions in Spike Protein	Geomean Neutralization IC_{50} (ng/mL)	Average Fold Change IC_{50} Relative to Reference[a]
I358	I358V, D614G	32.71	0.7
	I358L	44.01	0.8
	I358F, D614G	42.69	1.19
S359	S359N	95.55	0.96
	S359G, D614G	37.56	0.8
	S359R, D614G	62	0.89
	S359T, D614G	39.98	0.84
	S359I, D614G	38.01	0.84
N360	N360S, D614G	34.08	0.72
	N360Y, D614G	29.67	0.61
N440	N440D	80.47	1.29
	N440Y, D614G	42.65	0.68
	N440S, D614G	51.34	0.73
	N440K, D614G	19.99	0.48
	N440I, D614G	40.21	1.22
	N440T, D614G	50.81	0.82
	N440E, D614G	46.97	0.80
	N440F, D614G	43.07	0.85
L441	L441F, D614G	25.21	0.4
	L441I, D614G	32.96	0.7
	L441R, D614G	42.3	0.87
	L441V, D614G	48.24	0.98
	L441P, D614G	44.95	0.76